

1 Regional trends in the fractional solubility of Fe and other metals North 2 Atlantic aerosols (GEOTRACES cruises GA01 and GA03) following a 3 two-stage leach

4
5 Rachel U. Shelley^{1,2,3}, William M. Landing¹, Simon J. Ussher², Helene Planquette³, and Geraldine
6 Sarthou³

7 ¹Dept. Earth, Ocean and Atmospheric Science, Florida State University, 117 N Woodward Ave,
8 Tallahassee, Florida, 32301, USA

9 ²School of Geography, Earth and Environmental Sciences, University of Plymouth, Drake Circus,
10 Plymouth, PL4 8AA, UK

11 ³Laboratoire des Sciences de l'Environnement Marin, UMR 6539 LEMAR
12 (CNRS/UBO/IRD/IFREMER), Institut Universitaire Européen de la Mer, Technopôle Brest-Iroise,
13 Plouzané 29280, France

14
15 *Correspondence to:* Rachel U. Shelley (rshelley@fsu.edu)

16
17 **Abstract.** The fractional solubility of aerosol-derived trace elements deposited to the ocean surface is
18 a key parameter of many marine biogeochemical models. Yet, it is currently poorly constrained, in
19 part due to the complex interplay between the various processes that govern the solubilisation of
20 aerosol trace elements. In this study, we used a sequential two-stage leach to investigate the regional
21 variability in fractional solubility of a suite of aerosol trace elements (Al, Ti, Fe, Mn, Co, Ni, Cu, Zn,
22 Cd and Pb) from samples collected during three GEOTRACES cruises to the North Atlantic Ocean
23 (GA01, GA03-2010 and GA03-2011). We present aerosol trace element solubility data from two
24 sequential leaches that provide a “solubility window”, covering a conservative, lower limit to an upper
25 limit, the maximum potentially soluble fraction, and discuss why this upper limit of solubility could be
26 used as a proxy for the bioavailable fraction in some regions.

27 Regardless of the leaching solution used in this study (mild versus strong leach), the most heavily
28 loaded samples generally had the lowest solubility. However, there were exceptions. Manganese
29 fractional solubility was relatively uniform across the full range of atmospheric loading (32 ± 13 %
30 and 49 ± 13 % for ultra-high purity water and 25 % acetic acid leaches, respectively). This is
31 consistent with other marine aerosol studies. Zinc and Cd fractional solubility also appeared to be
32 independent of atmospheric loading. Although the average fractional solubilities of Zn and Cd (Zn: 37
33 ± 28 % and 55 ± 30 %, Cd: 39 ± 23 % and 58 ± 26 % for ultra-high purity water and 25 % acetic acid
34 leaches, respectively) were similar to Mn, the range was greater, with several samples being 100%
35 soluble after the second leach. Finally, as the objective of this study was to investigate the regional
36 variability in TE solubility, the samples were grouped according to air mass back trajectories
37 (AMBTs). However, we conclude that AMBTs are not sufficiently discriminating to identify the
38 aerosol sources or the potential effects of atmospheric processing on the physico-chemical
39 composition and solubility of the aerosols.

40 **1. Introduction**

41 Aerosol trace element (TE) solubility is a key parameter of many biogeochemical models, but it is
42 poorly constrained, e.g. Fe solubility estimates range from 0.001-90 % (Aguilar-Islas et al., 2010;
43 Baker et al., 2016). The fractional solubility (herein referred to as “solubility”) of aerosol TEs is
44 defined in terms of the amount of a TE in solution from any given leach that passes through a filter
45 (usually < 0.45 or 0.2 μm), expressed as a percentage of the total (Baker and Croot, 2010; Baker et al.,
46 2016; Jickells et al., 2016). While this operational definition accounts for some of the variability in
47 published values, it does not account for all of it. A number of factors impact aerosol TE solubility,
48 such as: (1) the choice of leaching protocol, and (2) the aerosol source, which in turn is impacted by a
49 combination of factors such as the mineralogy of the particles, atmospheric processing during
50 transport, and the presence/absence of emissions from e.g. vehicles, industry and agricultural
51 practices. Several studies have concluded that the most significant effects on aerosol Fe solubility
52 result from the source/composition of the aerosols, rather than changes in physico-chemical
53 parameters, such as temperature, pH and oxygen concentration of the leach medium, or the choice of
54 batch versus flow-through techniques (e.g. Aguilar-Islas et al., 2010; Fishwick et al., 2014).

55 There have been a number of studies that have focused on the role of aerosol TEs on biogeochemical
56 cycles in the North Atlantic (e.g. Sarthou et al., 2003; Baker et al., 2013; Buck et al., 2010; Ussher et
57 al., 2013; Powell et al., 2015). More recently, the GEOTRACES programme has produced a number
58 of aerosol datasets, which has stimulated further discussion on the use of this data to look for trends
59 that link TE solubility and aerosol source (e.g. Baker et al., 2016; Jickells et al., 2016). Elemental
60 ratios, enrichment factors and air mass back trajectory simulations have long been used as a first
61 approximation of aerosol source, and there are many studies that employ multivariate statistical
62 analyses for aerosol source apportionment (e.g. Chueinta et al., 2000; Laing et al., 2015). In addition,
63 more studies are making use of stable isotope ratios to investigate aerosol provenance. Some of these
64 methods are well-established and have a relatively long history of use in this purpose, such as Pb
65 isotopes (e.g. Maring et al., 1987), and Sr and Nd isotopes (e.g. Skonieczny et al., 2011; Scheuvs et
66 al., 2013 and references therein), and data from investigations of novel isotope systems are increasing.
67 For example, Fe isotopes show promise as a way to differentiate between anthropogenic and mineral
68 dust aerosols (Conway et al., submitted). In contrast, Cd isotopes may not be a suitable tool for aerosol
69 source apportionment (Bridgestock et al., 2017).

70 As the soluble fractions of aerosol TEs are thought to be the most-readily bioavailable forms (Shaked
71 and Lis, 2009), the leachable (soluble) fraction is used as a first approximation of the bioavailable
72 fraction. Therefore, experimental conditions should mimic natural conditions as closely as possible,
73 while yielding reproducible results. Ideally, the leach protocol used fits both these criteria. However,
74 that is not always strictly possible for reasons such as access to the leach medium of choice,

75 availability of analytical instrumentation, and cost. Currently, however, there is no standardised
76 aerosol leaching protocol, but it is recognised that this should be a priority for future studies (Baker et
77 al., 2016). Some commonly-used leach media are ultra-high purity (UHP) water (18.2 MΩ.cm),
78 seawater, weak acids (e.g. 1% HCl, 25 % acetic acid), or ammonium acetate buffer (e.g. Buck et al.,
79 2006, Baker et al., 2006b; Berger et al., 2008).

80 To investigate the regional variation in the solubility of key TEs in the North Atlantic, aerosol samples
81 were collected during the US-GEOTRACES GA03 campaigns in 2010 and 2011, and the French
82 GEOTRACES GA01 campaign in 2014 (www.geotraces.org). The focus of this paper is Fe and the
83 GEOTRACES “key” trace elements, Al, Cd, Cu, Mn, Pb, Zn, plus Co, Ni, and Ti (GEOTRACES
84 Planning Group, 2006). This suite of TEs includes bioactive elements, tracers of atmospheric
85 deposition, and elements characteristic of anthropogenic aerosols. Some TEs fit into more than one of
86 these categories. Here, we use the term ‘trace element’ in the context of open ocean water column
87 concentrations, thus acknowledging that elements such as Al, Fe and Ti are not present in trace
88 concentrations in aerosol source material. Aerosol concentrations for a suite of other elements (Li, Na,
89 Mg, P, Sc, V, As, Se, Rb, Sr, Sn, Sb, Cs, Ba, La, Ce, Nd, Th, U) were also determined, but will not be
90 discussed further here. However, these data are available at BCO-DMO (GA03; www.bco-dmo.org/)
91 and LEFE-CYBER (GA01; (www.obsvlfr.fr/proof/php/GEOVIDE/GEOVIDE.php), and on request
92 from the lead author.

93 In this study a two-stage leach protocol was followed. the first leach employed was the
94 “instantaneous” leach described by Buck et al. (2006) which is a flow-through method where the leach
95 medium is in contact with the aerosols for 10 - 30 s. It can be conducted using UHP water or seawater.
96 The advantages of using UHP water are that UHP water is a reproducible medium (allowing for inter-
97 lab comparisons) that can easily be analysed by ICP-MS for many elements simultaneously without
98 the need for time-consuming sample handling steps such as separation techniques and drying down
99 then re-dissolving the residue. Leaches with UHP water can be conducted at sea, or in the home
100 laboratory. If fresh sea water is used the leaches must be undertaken at sea.

101 Given that UHP water and rain water have broadly similar pH (~ pH 5.6), UHP water is used as an
102 analogue for rain/wet deposition, as wet deposition is thought to dominate the supply of many TEs, at
103 least at some regional and local scales (Helmers and Shremms, 1995; Kim et al., 1999; Powell et al.,
104 2015). However, the extremely low ionic strength of UHP water, and the absence of the metal binding
105 ligands naturally present in rain water and seawater (e.g. Chieze et al., 2012; Wozniak et al., 2014),
106 means that UHP water is not a perfect analogue for oceanic receiving waters. As such, freshly-
107 collected, filtered (< 0.2 μm) seawater likely produces a better estimate of the fractional solubility of
108 TEs on first contact with oceanic receiving waters. For Fe, leaches using UHP water (~ pH 5.6)

109 typically produce higher solubility estimates than leaches conducted with natural seawater (~ pH 8.2)
110 due to the pH sensitivity of dissolution and the higher ionic strength of sea water. On occasions where
111 higher solubility in seawater is observed, complexation by Fe binding ligands is likely the cause.
112 Regardless of whether UHP water or seawater is used, the instantaneous leach likely yields
113 conservative lower limit estimates of TE solubility due to the short contact time between the aerosols
114 and leach medium, and reports that aerosol solubility has a bi-modal behaviour for many TEs (initial
115 fast release, followed by a slower sustained release with time; e.g. Desboeufs et al. 2005; Kocak et al.,
116 2007; Mackey et al., 2015).

117 The second, sequential leach was employed in order to estimate an upper limit of TE solubility, and
118 provide a “solubility window”, but also as an estimate of the maximum bioavailable fraction during
119 the residence time of aerosol particles in the euphotic zone. We used the 25 % acetic acid leach with
120 hydroxylamine hydrochloride described by Berger et al. (2008). The pH of this leach (pH 2.1) is just
121 below that of zooplankton or fish digestive tracts and the reducing agent mimics the low oxygen
122 environments inside faecal pellets and marine snow aggregates. Indeed, Schmidt et al. (2016) have
123 demonstrated that lithogenic Fe is mobilised in the gut passage of krill resulting in threefold higher Fe
124 content in the muscle, and fivefold higher Fe content of the faecal pellets of specimens close to
125 lithogenic source material compared to those from offshore.

126 **2. Methods**

127 **2.1. Aerosol sample collection**

128 Aerosol samples (n = 57) were collected aboard the *R/V Knorr* during the *US-GEOTRACES GA03*
129 cruises (15 Oct – 2 Nov 2010 and 6 Nov – 9 Dec 2011, and aboard the *N/O Pourquoi Pas?* during the
130 French GEOTRACES GA01 cruise (GEOVIDE, 15 May – 30 June 2014) (Fig. 1). Both campaigns
131 took place in the North Atlantic Ocean, with GA03-2010 and GA01 departing from Lisbon, Portugal.
132 The cruise tracks were designed to traverse a wide variety of biogeochemical provinces (Longhurst,
133 2010) including; continental shelf regions, an eastern boundary current upwelling system (off West
134 Africa), the oligotrophic North Atlantic gyre, and sub-Arctic waters, and to span a large gradient in
135 atmospheric dust loading. The aerosol collections have been described previously (Wozniak et al.,
136 2013; 2014; Shelley et al., 2015; 2017). Briefly, air was simultaneously pulled through twelve acid-
137 washed 47 mm diameter Whatman 41 (W41) ashless filter discs at approximately $1.2 \text{ m}^3 \text{ min}^{-1}$ (134
138 cm s^{-1} face velocity) using a high-volume aerosol sampler (TSP model 5170V-BL, Tisch
139 Environmental). The metadata and concentration data for the aerosol leaches can be found in the
140 supplementary information (Table S1). All filters were stored frozen (-20°C) and double bagged prior
141 to processing, both on the ship and upon returning to the home laboratories.
142 To avoid contamination from the ship’s stack exhaust, aerosol sampling was controlled with respect to
143 wind sector and wind speed using an anemometer interfaced with a datalogger (CR800, Campbell

144 Scientific). The samplers were programmed to run when the wind was $\pm 60^\circ$ from the bow of the ship
145 and $> 0.5 \text{ m s}^{-1}$. When the wind failed to meet these two criteria, the motors were shut off
146 automatically and not allowed to restart until the wind met both the speed and direction criteria for 5
147 continuous minutes. In addition, the samplers were deployed on the ship's flying bridge as high off the
148 water as possible ($\sim 14 \text{ m}$ above sea level) to minimise collection of sea spray.

149

150 **2.2. Trace element determination – totals aerosol TEs**

151 The total digestion method of Morton et al. (2013) was used for the determination of total aerosol TE
152 loadings (Al, Ti, Mn, Fe, Co, Ni, Cu, Zn, Cd, Pb). The W41 filter discs were digested in tightly-
153 capped 15 mL Teflon-PFA vials (Savillex). Firstly, 1000 μL of ultrahigh purity (UHP) 15.8 M nitric
154 acid (Optima or Merck Ultrapur) was added to each vial, heated to 150°C on a hotplate, and then
155 taken to dryness. Secondly, 500 μL of 15.8 M nitric acid (13.2 M HNO_3) and 100 μL of 28.9 M
156 hydrofluoric acid (5.8 M HF) (Optima or Merck Ultrapur) was added to each vial, re-heated to 150°C
157 on a hotplate, then taken to near dryness. After the final digestion and evaporation step, the samples
158 were re-dissolved in 20 mL of 0.32 M nitric acid for analysis. All filter digestions were performed
159 under Class-100 laminar flow conditions. Total aerosol TE concentrations were determined by
160 magnetic sector field inductively coupled plasma mass spectrometry (ICP-MS; Thermo Element-2) at
161 the National High Magnetic Field Laboratory (NHMFL) at Florida State University (FSU; GA03) or
162 Pôle de Spectrométrie Océan (PSO) at the Institut Universitaire Européen de la Mer, France (IUEM;
163 GA01). Samples were introduced to a PFA-ST nebuliser (Elemental Scientific Inc.) via a modified
164 SC-Fast introduction system consisting of an SC-2 autosampler, a six-port valve and a vacuum rinsing
165 pump. Replicate blank solutions for the acid digestions were prepared by digesting W41 discs that had
166 been deployed in the aerosol samplers for 1 h while not in operation, and the resulting concentrations
167 were subtracted from all acid-digested filter samples. Details of the digestion blanks and analytical
168 figures of merit, including CRM recoveries, have previously been reported (Shelley et al., 2015;
169 2017).

170

171 **2.3. Trace element determination – soluble aerosol TEs**

172 In this study, we used a two-step, sequential leach to investigate regional variation in aerosol sources,
173 TE fractional solubility and bioavailability. We discuss the results from (1) an 'instantaneous' leach
174 (Buck et al., 2006), that provides a lower limit estimate of the most labile TE fraction (analogous to
175 the initial rapid release of TEs into rain drops and the surface mixed layer of the ocean), followed by
176 (2) a more protracted leach using 25 % acetic acid (with the reducing agent, hydroxylamine
177 hydrochloride, and heat, 10 min at 90°C), which mimics the slower and sustained release from aerosol
178 particles during their residence time in the euphotic zone.

179 The first step, the “instantaneous” leach, was conducted under a Class-100 laminar flow hood. In this
180 technique, 100 mL of UHP water ($> 18 \text{ M}\Omega\cdot\text{cm}$ resistivity, $\text{pH} \sim 5.5$, Barnstead Nanopure) is rapidly
181 passed through an aerosol-laden W41 filter held in a polysulfone vacuum filtration assembly
182 (Nalgene). Operationally-defined dissolved ($\leq 0.45 \mu\text{m}$) TEs are collected in the filtrate (leachate) by
183 positioning a GN-6 Metrice backing filter (cellulose esters) below the W41 disc in the filtration
184 assembly (Buck et al., 2006). In this study, the leachate was transferred to an acid-clean low density
185 polyethylene (LDPE) bottle and acidified to 0.024 M ($\sim \text{pH} 1.7$) with UHP HCl and double-bagged for
186 storage until analysis at FSU or IUEM. As for total elemental determinations, soluble TEs in the
187 leachate were also determined by ICP-MS. Leachate blanks were prepared by passing 100 mL of UHP
188 water through W41 filters that had been deployed in the aerosol sampler for 1 h while not in operation.
189 For example, leachate blanks for Fe represented an average of $1.6 \pm 0.4 \%$ and $15.5 \pm 15.8 \%$ of the Fe
190 sample concentrations for GA03 and GA01, respectively). A subset of samples (GA03-2011) were
191 also leached using the instantaneous leach procedure with freshly collected, filtered ($0.2 \mu\text{m}$) seawater
192 as the leach medium. Leachate blanks were subtracted from all leachate sample concentrations, details
193 of which can be found in Table S1 in the Supplementary Material.

194

195 The UHP water fractional solubility was calculated using Eq. (1):

196

$$\frac{[\textit{element}]_{\textit{UHP water leach}}}{[\textit{element}]_{\textit{total}}} * 100 = \textit{UHP water Fractional Solubility}$$

197

(1)

198 Following the instantaneous UHP water leach, the filter was transferred to a 15 mL centrifuge tube,
199 and the second leach was undertaken, using 5 mL of 25 % (4.4 M) ultrapure acetic acid, with 0.02 M
200 hydroxylamine hydrochloride as the reducing agent (Berger et al., 2008). After a 10 min heating step
201 ($90 \text{ }^\circ\text{C}$), the leaches were left for 24 h before being centrifuged for 5 min at 3400xg . The leachate was
202 then carefully decanted into acid-clean LDPE bottles. In order to rinse any residual acetic acid from
203 the filter, 5 mL of UHP water was pipetted into the centrifuge tubes, which were then centrifuged
204 again for 5 min at 3400xg . This supernatant was then added to the acetic acid leachate in the LDPE
205 sample bottles. As this second leach aims to access a less labile fraction of the TEs of interest
206 (including TEs absorbed to surfaces, TE oxyhydroxides and TEs complexed by aerosol organic
207 matter), without significantly attacking TEs bound within the mineral matrix (Koçak et al., 2007;
208 Berger et al., 2008), it may provide an upper limit estimate for the fractional solubility of these aerosol
209 TEs as the aerosols mix down into the ocean. There is a slight risk that the heating step could begin to
210 attack the mineral matrix, resulting in a slight over-estimation of the upper limit of solubility, but this
211 risk was shown to be minimal (Berger et al., 2008). Despite this risk, the heating step was included
212 because of the desire for procedural similarity with marine particle leaches from the same cruises (e.g.
213 Planquette et al., 2016; H. Planquette and A. Gourain pers. comm.), which have been used to assess

214 the relative importance of atmospheric inputs of TEs to water column concentrations of Al, Fe and Pb
215 (Menzel-Baraqueta et al.; Tonnard et al.; Zurbrick et al., this issue).

216 As all samples in this study were leached first using the UHP water instantaneous leach, followed by a
217 sequential leach with 25 % acetic acid, the overall solubility in 25% acetic acid was calculated using
218 Eq. (2):

$$\frac{[element]_{UHP\ water\ leach}}{[element]_{total}} + \frac{[element]_{25\% \ HAc\ leach}}{[element]_{total}} * 100 = HAc\ Fractional\ Solubility \quad (2)$$

221 **2.4. Major anion determination**

222 Before the UHP water leachate was acidified, a 10 mL aliquot was taken from each leach sample for
223 the determination of the soluble major anions. The aliquot was immediately frozen for storage. The
224 anions, Cl⁻, NO₃⁻ and SO₄²⁻, were determined by ion chromatography using either a Dionex 4500i (at
225 FSU for GA03 samples) or a Metrohm, IC850 system (at Laboratoire Interuniversitaire des Systèmes
226 Atmosphériques, Paris for GA01 samples).

227

228 **2.5. Air mass back trajectory simulations**

229 Air mass back trajectory (AMBT) simulations were generated using the publicly-available NOAA Air
230 Resources Laboratory Hybrid Single-Particle Lagrangian Integrated Trajectory (HYSPLIT) model,
231 using the GDAS meteorology (Stein et al., 2015; Rolph, 2017). The 5-day AMBT simulations were
232 used to describe five regional categories, based on the predominant trajectories for the air masses. The
233 simulations and further details of these categories can be found in Wozniak et al., (2013; 2014) and
234 Shelley et al., (2015; 2017). Briefly, for cruise GA03 air masses were characterised as European,
235 North American, North African, or Marine (no or minimal interaction with major continental land
236 masses within the 5-day simulation period). For cruise GA01, all the samples were classified as High
237 Latitude dust (originating north of 50°N; Bullard et al., 2016). The classifications are shown in Table
238 S1, and the AMBT simulations from Shelley et al. (2015; 2017) have been reproduced and can be
239 found in the Supplementary Material (Fig. S1). The simulations use arrival heights of 50, 500 and
240 1500 m, so that at least one height was located in the marine boundary layer.

241

242 **3. Results and Discussion**

243 **3.1. Identifying aerosol provenance**

244 Air mass back trajectory (AMBT) simulations are frequently used to identify the origin and/or flow
245 path of air masses, from which a first approximation of aerosol provenance (e.g. deserts, urban
246 regions, or biomass burning) are made. While a useful tool in oceanographic studies, AMBTs used

247 alone do have limitations. Perhaps the most significant of these is that they are unable to quantify the
248 contribution of different aerosol types or the entrainment of particles along the flow path of the air
249 mass. Indeed, within the five categories described in this study multiple sources are likely to have
250 contributed to the composition of the bulk aerosol of each category. This study is likely to be
251 particularly sensitive to this as the sampling site was not static (i.e. sampling occurred along three
252 different transects), and air masses can, and do, take different pathways within a general wind
253 direction. Consequently, AMBTs are not adequately discriminating for aerosol source apportionment.
254 However, we have organised the data using the AMBT categories as the objective of this study was to
255 look for trends in solubility at a regional level, and also for consistency with our earlier published
256 work from the North Atlantic (Wozniak et al., 2013; 2014; Shelley et al., 2015; 2017).

257 More powerful approaches for aerosol source apportionment consider the physico-chemical
258 composition of the aerosols, either as the bulk aerosol or individual particles. There have been a
259 number of field campaigns (e.g. DABEX, DODO, SAMUM and AMMA) and individual studies
260 which have provided a wealth of information about the physico-chemical composition of African dust
261 before, during and after long-range transport (e.g. Johansen et al., 2000; Johnson et al., 2008;
262 McConnell et al., 2008; Petzold et al., 2009; Marticorena et al., 2010; Trapp et al., 2010; Formenti et
263 al., 2011). These studies, and satellite data have identified the key dust source regions in North Africa
264 (Prospero et al., 2002). Chemical composition data for other aerosol end members which supply
265 aerosols to the North Atlantic is not as extensive, but some examples of individual studies and field
266 campaigns can be found in Table S2. In addition, campaigns in the Atlantic Ocean which have
267 sampled marine aerosols (e.g. Atlantic Meridional Transect, CLIVAR, GEOTRACES) have identified
268 aerosol sources from characteristic groups of elements and elemental ratios (e.g. high concentrations
269 of lithogenic elements are characteristic of a mineral dust, K is a tracer of biomass burning, and
270 correlations between V and Ni are diagnostic of emissions from marine shipping; Baker et al., 2006a;
271 Sippula et al., 2014; Baker and Jickells, 2017), organic composition (e.g. Wozniak et al., 2013; 2014,
272 2015), and/or stable isotopic signatures (Scheuvens et al., 2013 and references therein).

273 Although atmospheric inputs to the ocean are episodic and exhibit a seasonality in the tropical and
274 subtropical North Atlantic that is largely driven by the migration of the intertropical convergence zone
275 (Prospero et al., 1981; Adams et al., 2012; Doherty et al., 2014), North African/Saharan mineral dust
276 dominated the aerosol composition in the GA03 study region (Conway and John, 2014; Shelley et al.,
277 2015; Conway et al., submitted). Other aerosol sources in Europe and North America and sea salt also
278 contributed to the bulk aerosol to varying extents. In contrast to GA03, the GA01 transect was located
279 north of the extent of the Saharan dust plume ($\sim 25^\circ$ N in summer, Ben-Ami et al., 2009), and was
280 thus influenced by a mixture of high latitude dust sources (Prospero et al., 2012; Shelley et al., 2017),
281 which also have a seasonal cycle. As a result, a large dynamic range of aerosol loading was observed

282 (Fe = 0.185–5650 ng m⁻³; Al = 0.761- 7490 ng m⁻³) during these two campaigns, with the highest Fe
283 and Al loadings associated with the North African samples (GA03), lower loadings with the Marine
284 samples (GA03), and the lowest loadings observed in the samples collected in the Labrador Sea
285 (GA01).

286 Total Fe and Al were strongly correlated ($r^2 = 0.999$, Pearson's ρ $P < 0.01$), demonstrating that the two
287 metals have common lithogenic source(s) (Fig. 2). However, this correlation was largely driven by the
288 heavily-loaded North African samples ($r^2 = 0.997$, $P < 0.01$). For each of the other source categories,
289 simple linear regression of the data resulted in r^2 values of: 0.879 ($P < 0.01$) for High Latitude dust
290 (GA01), 0.890 ($P = 0.057$) for European samples (GA03), 0.983 ($P = 0.34$) for N. American samples
291 (GA03) and 0.751 ($P = 0.70$) for Marine samples (GA03) (Fig. 2b). Further discussion of sub-regional
292 differences in the Fe/Al ratio are addressed later in the Discussion. For the other TEs, strong
293 correlations for the combined GA01 and GA03 datasets were found between Ti/Al ($r^2 = 0.999$, $P <$
294 0.01), Mn/Al ($r^2 = 0.994$, $P < 0.01$) and Co/Al ($r^2 = 0.996$, $P < 0.01$), in accord with previous
295 observations in this region owing to the primarily lithogenic sources of these elements (e.g. Jickells et
296 al., 2016). The correlations between Al and the primarily anthropogenic TEs, Ni, Cu, Zn, Cd, and Pb,
297 were also significant at the 99% confidence level : Ni/Al ($r^2 = 0.884$), Cu/Al ($r^2 = 0.652$), Pb/Al ($r^2 =$
298 0.478), Zn/Al ($r^2 = 0.321$), Cd/Al ($r^2 = 0.303$) due the presence of the heavily-loaded North African
299 samples , which accounted for between 88 % and 30 % of the statistical variance for Ni and Cd,
300 respectively. Sources other than mineral dust (e.g. metal smelting emissions, fly ash, vehicle
301 emissions, volcanic ash, proglacial till) are presumably responsible for the residual variance.
302 Establishing the contributions from these other aerosol sources and their influence on TE solubility is
303 a research priority.

304 As the aerosol source has a direct bearing on the type and composition of aerosols, determining the
305 source could provide useful data that might be used to predict the fractional solubility of aerosol TEs.
306 As positive matrix factorisation (PMF) can be used for source apportionment, we used the USA
307 Environmental Protection Agency's EPA PMF model (v. 5.0) with the total TE concentration data to
308 look for trends in the data. However, the GA01 and GA03 dataset is relatively small ($n = 57$) and the
309 model was not stable with more than two factors. The two factors were a mineral dust factor (high
310 contributions from lithogenic TEs, in particular Al, Ti, Fe and Zr) and a pollution/anthropogenic factor
311 (with high contributions from Zn and Pb) (Fig. S2a, Supplementary Material). As anticipated, the
312 mineral dust factor dominated where North African aerosols were sampled, and the pollution factor
313 was relatively more important closer to the European and North American continents (Fig. S2b). This
314 is in accord with the samples from North Africa having elemental mass ratios that are consistently the
315 closest to the UCC elemental ratios compared to aerosols from the other source regions (Fig. 3). In
316 the High Latitude samples, the pollution factor and the mineral dust factor were of approximately

317 equal dominance. Interestingly, the North African aerosols also contained a relatively strong pollution
318 component, consistent with a northeast flow into North Africa from Europe, followed by entrainment
319 of mineral dust during passage over the Sahara (Baker and Jickells, 2017). Given that the PMF
320 indicates that 100 % of the variability in the Cd concentrations was explained by the pollution factor,
321 this suggests that Cd in North African aerosols is not sourced from mineral dust, which would explain
322 why no fractionation was observed in Cd isotopes from North African and European aerosols
323 (Bridgestock et al., 2017). Further, it also suggests that even the relatively homogeneous aerosols from
324 North Africa do not represent a ‘pure’ end-member. However, the PMF analysis was not sensitive
325 enough to identify the full complement of aerosol sources contributing to the samples collected during
326 GA01 and GA03.

327 **3.2. Elemental mass ratios and aerosol source**

328 Elemental mass ratios from the ten most heavily loaded GA03 North African aerosols were averaged
329 to derive a value for the ‘North African’ ratio depicted by the dashed horizontal line in Figures 3(a-i).
330 Aluminium was used to normalise the data (Fig. 3; Table S2) and was chosen instead of Ti, another
331 proxy for mineral dust, due to the presence of some anomalously high Ti/Al ratios in some of the
332 Marine samples during GA03 (Fig. 3a; Shelley et al., 2015). We have previously reported a mass ratio
333 of 0.76 for Fe/Al for the North African end-member aerosols (Shelley et al., 2015; Fig. 2a), which is
334 significantly higher than the mean upper continental crustal (UCC) ratio of 0.47 (Rudnick and Gao,
335 2003) but entirely consistent other studies of Saharan soils and dust (e.g. Chiapello et al., 1997; Guieu
336 et al., 2002; Lafon et al., 2006; Baker et al., 2013).

337 For North African dust there does not appear to be a discernible source dependent trend in Fe/Al ratios
338 due to a natural variability in Fe-bearing minerals in soils in dust source regions (Lafon et al., 2006;
339 Scheuven et al., 2013), but it might be possible to use Fe/Al ratios for some of the other aerosol
340 groups to suggest different sources. For example, the European samples (n = 4) fall into two sub-
341 groups: two samples have low Fe/Al ratios (Fig. 2; E3 = 0.48, E4 = 0.10 and Fig. 3c), whereas the
342 other two samples (E1 = 0.95 and E2 = 0.78) have Fe/Al ratios within the range of the North American
343 samples (Fe/Al 1.1 ± 0.22 , range 0.86-1.42) and all but one of the Marine samples (Fe/Al, excluding
344 M12, 0.93 ± 0.33 , range 0.59-1.61; M12, collected closest to the North African samples, Fe/Al =
345 0.43).

346 Aerosols from the more northerly section, GA01, were largely outside the influence of the Saharan
347 dust plume (Shelley et al., 2017), and are all classified as High Latitude in this study (Fig. 3). For this
348 group of samples, there were also sub-groups of Fe/Al ratios. During the first half of the cruise (Fig.
349 1), there was a group of samples (G1-6, G8 and G10) with Fe/Al ratios of 0.58 ± 0.05 ; Fig.3c). This is
350 intermediate between the UCC ratio (0.48 ± 0.07) and the North African mineral dust ratio ($0.78 \pm$

0.03; Fig. 3c). For these samples, the wind direction was predominantly from the north/north west (Shelley et al., 2017), so it is unlikely that the observed ratios reflect a mixture of North African mineral dust and European aerosols. Rather, it more likely comes from high latitude sources, as dust supplied by proglacial till from Iceland and Greenland peaks in spring/early summer, and can be deposited over the Atlantic Ocean (Prospero et al., 2012; Bullard et al., 2016). Unfortunately, the extensive cloud cover experienced during the GA01 cruise (May/June 2014) prevented the use of satellite observations (e.g. <http://worldview.earthdata.nasa.gov>) which would have confirmed the presence of dust from these sources. The elemental ratios calculated from TE concentrations from volcanic ash sampled during the eruption of the Eyjafjallajökull volcano in 2010 (Achterberg et al., 2013) offers some limited support for this argument, as our range of elemental ratios encompasses this end-member (Icelandic soils are almost exclusively volcanic in origin; Arnalds 2004). However, although Icelandic sands (Baratoux et al., 2011) and tephra (Oladottir et al., 2011) have Mn/Al ratios that overlap the GA01 samples, Fe/Al is generally lower in our High Latitude dust samples (Table S2).

A second group of GA01 samples (G7, G9, G11 and G12) had Fe/Al ratios of 0.34 ± 0.01 , but no obvious link in terms of the AMBTs. The Greenland shelf and Labrador Sea samples, except G15, had low Fe/Al (0.16 ± 0.04), and were distinct from those collected on the Canadian shelf (0.48 ± 0.02). These trends strongly suggest that the High Latitude dust was made up of at least four aerosol sources.

While there is evidence for anthropogenic source(s) of aerosol Fe to the North Atlantic (Conway et al., submitted), which is more soluble than Fe associated with mineral dust (Sedwick et al., 2007; Sholkovitz et al., 2009; 2012), North African mineral dust dominates the supply of Fe to much of the study region (Baker et al., 2013; Shelley et al., 2015; 2017; Conway et al., submitted). In addition to the samples classified as European and North American, elevated Fe/Al ratios were also observed in the Marine samples (Fig. 2b). In addition to aerosols derived from continental sources (meaning either mineral dust or anthropogenic emissions), sea spray aerosols could make a relatively higher contribution to the bulk aerosol in remote oceanic locations (de Leeuw et al., 2014). However, this would have the opposite effect as the ratio of Fe/Al in surface seawater ($0.017 - 0.024$ in the North Atlantic gyre, 0.019 European continental shelf, and $0.030 - 0.031$ in the Mauritanian upwelling zone; Hatta et al., 2015) is two orders of magnitude lower than the crustal ratio. Hence the contribution of sea spray aerosols appears to have a negligible impact on the Fe/Al ratios in the bulk Marine aerosols.

The Marine, and the High Latitude samples had the widest range in Fe/Al ratios and were also collected in the most remote locations. These groups also had the greatest difference in the Fe/Al ratios between the total and soluble fractions, and also contained the samples with the lowest ratios of Fe/Al in the soluble fraction (minimum Fe/Al = 0.15 , samples G9-GA01 and M3-GA03; Fig. 3c), suggesting that even though aerosol Fe is altered towards more soluble forms during atmospheric

385 transport (Longo et al., 2016), atmospheric processing renders Al even more soluble relative to Fe.
386 However, although the soluble ratio of Fe/Al was the same for samples G9-GA01 and M3-GA03, the
387 fractional solubility for Fe differed from 20 % for G9-GA01 to 0.8 % for M3-GA03. We suggest that
388 North African mineral dust was contributing to the composition of M3-GA03, resulting in the low
389 solubility of Fe compared to G9-GA01. This suggestion is supported by isotopic evidence (Conway et
390 al., submitted).

391 For the anthropogenically-derived TEs, Ni, Cu, Zn, Cd and Pb (Figs. 3e-i) and for at least some of
392 samples of the mixed-source TEs (i.e. having crustal and pollution sources; e.g. Mn and Co in Figs. 3b
393 and d), there is some degree of source-dependence in the elemental ratios, with some significant
394 increases from the UCC mass ratios in the total (Shelley et al., 2015) and UHP water soluble fractions
395 (Fig. 3). The higher ratios of the UHP water soluble fraction compared to the total indicates that these
396 TEs are more labile than Al. In addition, studies that have investigated the size distribution of aerosols
397 have found that anthropogenically-derived TEs tend to be associated with fine mode aerosols (< 1 μm
398 diameter), which are more soluble than coarse mode aerosols due to the larger surface area to volume
399 ratio (Duce et al., 1991; Baker and Jickells 2006; Baker and Jickells, 2017). Size fractionated samples
400 were collected during the GA03 cruise, and the smaller size fractions were indeed more soluble than
401 the larger ones for Al, Fe and Co (Landing and Shelley, 2013). Enrichment of TEs with predominantly
402 anthropogenic sources accords with other studies in the North Atlantic, and is most striking for
403 aerosols that did not originate from the sparsely-populated, arid regions of North Africa (e.g. Buck et
404 al., 2010; Gelado-Cabellero et al., 2012; Patey et al., 2015; Shelley et al., 2015).

405

406 **3.3. Aerosol solubility**

407 **3.3.1. Solubility of aerosol TEs as a function of total concentration: UHP water (instantaneous)** 408 **compared to 25 % acetic acid leaches**

409 The UHP water soluble fraction of aerosol Fe and Al determined for all the North Atlantic GA01 and
410 GA03 samples varied by two orders of magnitude (Fig. 4a: Fe = 0.14 - 21 %, median 2.2 %; Al = 0.34
411 - 28 %, median 2.7%). Although a broader range of Fe and Al solubility was observed in this study,
412 both these results and those reported by Buck et al. (2010) using the same approach (Fe = 2.9 - 47%,
413 median = 14%, and Al = 3.7 - 50%, median = 9.5%) broadly agree that the median UHP water soluble
414 fractions of Fe compared to Al in the North Atlantic are similar. While there was considerable overlap
415 in the ranges of fractional solubility of TEs in aerosols from the different regions (e.g. Fe: European
416 1.9 – 21 %; N. American 0.84 – 8.8 %; Marine 1.7 – 18 %; High Latitude dust 1.9 – 20 %), the North
417 African samples, identified by their orange colour, high Fe and Al loadings, and definitive AMBTs)
418 formed a distinct cluster of very poorly soluble Fe, or Al (< 1%; Fig. 4a). However, the solubility of
419 the North African ('Saharan') aerosol Fe was 1 – 2 orders of magnitude lower in this study (0.14 –

420 0.57 %) than during the Buck et al. (2010) study (2.9 – 19 %). This supports the hypothesis that TEs
421 from North African aerosols sampled closer to the source (as in this study) are less soluble due to a
422 lesser degree of atmospheric processing and/or larger particle sizes (Baker and Jickells, 2006; Longo
423 et al., 2016).

424 The inverse relationship between total aerosol loading and fractional solubility has previously been
425 reported for Fe (Sholkovitz et al., 2009; 2012; Jickells et al., 2016) and Al (Jickells et al., 2016).
426 Jickells et al. (2016) compiled solubility data from the North Atlantic and found that the general trend
427 between Fe and Al solubility and atmospheric loading was robust over the range of atmospheric
428 loadings found in the North Atlantic, regardless of the leach protocol employed. In this study, both the
429 UHP soluble, and 25 % acetic acid soluble fractions of Fe and Al (Figs 4a and b) were related to
430 atmospheric loading, i.e. the highest loaded North African samples had the lowest solubility. The
431 possible exception to this trend is the fraction of Al that dissolved from North African aerosols
432 following the 25 % acetic acid leach (Fig. 4b). However, it could simply be that we are observing
433 scatter in our data, which is smoothed out in the larger dataset ($n > 2000$) examined by Jickells et al.
434 (2016). Although, we cannot rule out that this effect is the result of the heating step in the 25 % acetic
435 acid leach attacking the alumino-silicate matrix, the similarity in the trend of the solubility of Ti in
436 UHP water and 25 % acetic acid (sharp decrease in solubility with increased aerosol loading, Figs. 4a
437 and b) suggests that matrix attack is minimal. Further experimentation with and without the heating
438 step would help to clarify this issue.

439 Aluminium, Ti, and Fe show very similar behaviour in Figure 4a (sharply decreasing solubility as
440 loading increases). Cobalt, Ni, Cu, Zn and Pb solubilities decrease less strongly as loading increases,
441 whereas Mn and Cd show no clear trend. For the acetic acid leaches (Fig. 4b), Ti follows the same
442 trend as the UHP water leach (Fig. 4a), while Al and Fe plateau at 8-10 % solubility. The other TEs
443 (Mn, Co, Ni, Cu, Zn, Cd and Pb) all show almost no trend with loading. The absence of an inverse
444 trend between solubility and loading has previously been noted for Mn (Jickells et al., 2016). For Co
445 the inverse relationship between UHP water solubility and loading was not observed when using the
446 25 % acetic acid leach, most likely because Co may be associated with the Mn and Fe oxides that are
447 easily reduced using this leach. For Zn and Cd, although their average fractional solubilities (Zn: $37 \pm$
448 28% and $55 \pm 30 \%$, Cd: $39 \pm 23 \%$ and $58 \pm 26 \%$ for ultra-high purity water and 25 % acetic acid
449 leaches, respectively) were similar to Mn ($32 \pm 13 \%$ and $49 \pm 13 \%$ for ultra-high purity water and 25
450 % acetic acid leaches, respectively), the range was greater, with several samples from different regions
451 (although not North Africa) being 100% soluble after the second leach.

452 **3.3.2. Solubility of TEs: UHP water (instantaneous) compared to 25 % acetic acid leaches**

453 All ten TEs from the five different provenances were less soluble in UHP water than 25 % acetic acid
454 (Fig. 5). This is not a surprising finding given the lower pH of acetic acid compared with UHP water,
455 acetate being a bidentate ligand, the longer contact time of the aerosols with the leach solution, the
456 addition of the hydroxylamine reducing agent and that the fractional solubility of TEs in 25 % acetic
457 acid was calculated using Equation 2 (which sums the UHP water and 25 % acetic acid leach
458 concentrations). In addition, there is some degree of source-dependent variability in the relative
459 proportions of each TE that is released by the two leaches. In general, as with the leaches with UHP
460 water, the North African aerosols were distinctly less soluble in 25% HAc compared with aerosols
461 from the other source regions (Fig. 5). Figure 5 highlights the distinction between the lithogenic
462 elements, Al, Fe and Ti, which have uniformly low solubility in UHP water (mostly < 20 %), and
463 extremely low solubility in North African aerosols (< 1 %), and the anthropogenic, pollution-
464 dominated elements, Ni, Cu, Zn, Cd and Pb which have solubility up to 100 %. Manganese (Mn) and
465 Co have both lithogenic and anthropogenic sources, so are classified as “mixed-source”, and have
466 intermediate solubilities. Like all the TEs reported here, Mn solubility in UHP water was significantly
467 less ($p < 0.01$, two-tailed, homoscedastic t-test) in North African aerosols (median solubility = 19 %)
468 than in the non-North African samples (median = 38%), which seems to contrast somewhat with the
469 findings of Baker et al. (2006b) and Jickells et al. (2016) which found that aerosol source had little
470 impact on Mn solubility. However, in common with these earlier studies (Baker et al., 2006b; Jickells
471 et al., 2016), there was no significant source-dependent difference in Mn solubility in 25 % acetic acid
472 (non-North African samples: $49 \pm 15\%$, North African samples: $49 \pm 6.4\%$).

473 **3.3.3. Soluble TEs: UHP water compared to seawater instantaneous leaches**

474 Seawater leaches were conducted on a subset of samples (GA03-2011), to investigate the suitability of
475 seawater as the leach medium in the instantaneous leach (Fig. 6). During this study, Fe solubility in
476 seawater was lower than in UHP water (Fig. 6c). This phenomenon has previously been observed in
477 atmospheric aerosols from the North Atlantic Ocean (Buck et al., 2010). For Fe, only a few samples
478 of North American and Marine provenance conformed to the relationship described by the equation
479 proposed by Buck et al. (2010), with most of our data plotting above the regression line of the Buck et
480 al. (2010) study (Fig. 6c), indicating that our data was relatively more soluble in UHP water compared
481 to seawater than in this earlier study. One possibility is that the higher aerosol Fe loadings we
482 observed during GA03-2011 (this study, maximum = $5650 \text{ ng Fe m}^{-3}$), compared to the A16N-2003
483 transect (Buck et al. 2010; maximum = $1330 \text{ ng Fe m}^{-3}$), resulted in a particle concentration effect
484 (Baker and Jickells, 2006), whereby the relationship between aerosol Fe loading and fractional
485 solubility breaks down because dust on the filter can be a source of soluble Fe but can also scavenge
486 dissolved Fe from the sea water leach solution as it passes through the filter. Given that the link
487 between Fe solubility in seawater and Fe-binding ligand availability is well established (e.g. Rue and

488 Bruland, 1995; Gledhill and Buck, 2012), an alternative explanation for the difference in Fe solubility
489 is that the organic composition of the seawater used as the leach mediums differed between the two
490 studies.

491 Manganese is the only TE that had a slope close to unity (0.98; Fig. 6b), suggesting that solubility
492 estimates were not impacted by the choice of leach medium used. This is consistent with other studies
493 that have found that Mn solubility is less sensitive to the choice of leach media, or to aerosol
494 provenance than other TEs (Baker et al., 2006b; Jickells et al., 2016). Due to the large variability in
495 the data set, there was no significant difference between Mn solubility in UHP water or seawater ($32 \pm$
496 13% and $24 \pm 17 \%$, respectively; Fig. S3 and Tables S3 and S4, Supplementary Material). Table S5
497 shows which regions had slopes for UHP water versus seawater fractional solubility that did not differ
498 significantly from 1.0 at the 95 % confidence level (t-statistic).

499 Lead was the only TE with all slopes differing significantly from 1.0, and the only TE where the
500 solubility in seawater was higher than in UHP water for virtually every sample (Fig. 6i). As for Pb,
501 most of the Co data falls below the 1:1 line (Fig. 6d), indicating that Co was also generally more
502 soluble in seawater than UHP water. In contrast, the opposite trend was observed for Fe and Ni (Figs
503 6c and e), perhaps due to differences in the availability of metal binding ligands in the seawater used.
504 A challenge of using seawater as the leach medium is that it is difficult to control for natural
505 variability in the types and concentrations of organic ligands. Consequently, it is not possible to
506 determine conclusively why contrasting trends in the fractional solubility of TEs were observed. For
507 this reason, we advocate for the use of UHP water as a common leach medium to facilitate
508 comparisons of solubility resulting from differences in aerosol composition. An additional benefit is
509 the ease of analysis of UHP water compared to seawater.

510

511 **3.4. Visualising marine aerosol sources using multivariate statistical approaches**

512 As the PMF analysis was only able to identify two significant factors accounting for the total aerosol
513 TE concentrations, another multivariate approach was taken. Hierarchical cluster analysis (Ward's
514 method, Euclidian distance) was performed using the R statistical package (v. 3.3.0; R Core Team,
515 2016) to look for trends in the data that might reveal the various aerosol sources. Hierarchical cluster
516 analysis was performed on (1) log transformed total aerosol TE plus NO_3^- concentration data (Fig. 7a),
517 and (2) log transformed TE fractional solubility plus NO_3^- concentration data (Fig. 7b). The NO_3^-
518 concentrations appear in both runs as we wanted to include TEs plus an indicator of anthropogenic
519 pollution.

520 Figure 7a shows two main branches to the dendrogram of the total TE concentration data. One branch
521 groups all the North African and European samples and two North American samples (N2 and N4)
522 together, and the other branch groups all other samples together. Samples closest to each other are the
523 most similar to each other, and those joined in the same groups share similar characteristics.
524 Therefore, in this analysis, the North African samples are grouped together, as are the High Latitude
525 samples. All but three North African samples form a distinct sub-group. The three remaining North
526 African samples (A8, A9 and A11) share more characteristics with the European samples, lending
527 support for mixing of aerosols from the two regions. Counterintuitively, the two European samples
528 with the lowest Fe/Al ratios (E3 and E4) are the ones that are most similar to the two North American
529 samples, which have relatively high Fe/Al ratios of 0.90 and 0.87. The GA01 samples (with the
530 exception of one sample, G15) form a distinct cluster, but with three sub-groups: one is the
531 Greenland/Labrador Sea samples (without G15), and the other two are related to each other but
532 distinct from the Greenland/Labrador Sea samples and are a mixture geographically of the other
533 samples. However, there is a trend, the 'middle' group is the group of samples collected closest to land,
534 the group to the right is the group of samples collected furthest from land. The other groupings are
535 made up of a mixture of North American and Marine samples. This could suggest that the Marine
536 samples are comprised predominantly of North American aerosols from more than one source. The
537 only anomaly is the two North American samples that 'look European'.

538 Although there are differences between Figures 7a (total TEs) and 7b (25 % acetic acid fractional
539 solubility; Eq. 2), the general trend of an inverse relationship between TE atmospheric loading and
540 fractional solubility holds, as the North African samples with the highest concentrations and lowest
541 fractional solubilities appear on the left in Figure 7a, and on the right in Figure 7b. In terms of
542 fractional solubility, the N. African samples form a distinct cluster, but this cluster is made up of two
543 sub-groups: one collected during GA03-2010 and one during GA03-2011. The samples from near
544 Greenland and the Labrador Sea are also distinct from the other GA01 samples (again with the
545 exception of G15), and also distinct from all other samples. The European samples, all other GA01
546 samples, and three North American samples form a loose cluster. The remaining North American
547 samples and all the Marine samples form another loose cluster.

548 Plotting the data this way still does not allow us to identify the aerosol sources definitively, but it does
549 allow us to visualise which samples have the most similar physico-chemical characteristics and
550 confirms the general trend of a relationship between aerosol loading and fractional solubility and, by
551 extension, bioavailability, even though we have demonstrated that this relationship is not present for
552 all TEs. This knowledge is then useful as a general rule of thumb in biogeochemical models, although
553 clearly other factors also exert controls on aerosol TE solubility. For example, during their
554 investigations of the GA03 aerosols, Wozniak et al., (2013; 2014; 2015) proposed a role for water

555 soluble organic carbon (WSOC) in controlling the solubility of Fe. Desboeufs et al. (2005) also found
556 evidence for a link between total carbon and TE solubility in regions impacted by anthropogenic
557 activity. Thus, the carbon content of aerosols is also implicated as a control on aerosol Fe solubility,
558 but the relationship is frequently not linear.

559

560 **3.5. Choice of leach and modelling TE solubility**

561 The ability of models to replicate subtleties in aerosol TE solubility may prove critical in forecasting
562 ecosystem impacts and responses. Due to the magnitude of North African dust inputs to the North
563 Atlantic region (very high dust inputs result in a high soluble aerosol TE flux despite relatively low
564 fractional solubility), this is a particular challenge and is compounded by additional unknowns such as
565 how aerosol acidity will be impacted by the combined effects of increasing
566 industrialisation/urbanisation, and changes in the magnitude of future mineral dust supply and biomass
567 burning (Knippertz et al., 2015; Weber et al., 2016). In other words, it is important to accurately
568 constrain aerosol trace element solubility with high quality data in order to improve the predictive
569 capacity of models. Clearly the choice of leach media and protocol impacts the measured fractional
570 solubility. This is shown in both Figures 4 and 5 and has a number of implications with regard to
571 modelling the impact of atmospheric deposition on marine biogeochemistry. For example, for
572 elements with generally low solubility, such as Fe, the difference between 1 % and 2 % solubility is an
573 increase of 100 %, meaning that only half the amount of dust is needed to yield the same amount of
574 dissolved Fe. To complicate matters further, recent research has demonstrated that some diazotrophs
575 are able to directly access particulate Fe (Rubin et al., 2011). The significance of this is that
576 *Trichodesmium* are common in the North Atlantic gyre under the influence of the Saharan plume, and
577 the North African dust samples have higher fractional solubility for Fe using the acetic acid leach. If
578 *Trichodesmium* are able to access the acetic acid soluble fraction of the aerosol Fe, as the study
579 indicates (Rubin et al., 2011), our data suggests that twentyfold more aerosol Fe is available for uptake
580 than is suggested from the instantaneous UHP water leach. This suggests that in regions where
581 *Trichodesmium* proliferate, we are likely to underestimate bioavailable Fe using the instantaneous
582 UHP water leaching method.

583 There are implications for modelling the impact of atmospheric deposition for other TEs. Although,
584 the lack of source dependent differences in Mn solubility in these aerosols makes modelling Mn
585 solubility simpler, there was still a difference in the fractional solubility calculated from the two
586 leaches (UHP water: 32 ± 13 % and 25 % acetic acid: 49 ± 13 %). However, for Al, there was a large
587 range in solubility: 0.3 – 28 % using UHP water and 4.1 – 100 % using 25 % acetic acid. Both ranges
588 far exceed the relatively narrow range used in the MADCOW model (1.5 – 5 %), which has been used

589 to estimate atmospheric inputs based on dissolved Al concentrations in the mixed layer (Measures and
590 Brown, 1996). It is noted, however, that the median values from this study fall within the range used
591 by the MADCOW model (2.7 % and 3.3 % for UHP water and 25 % acetic acid, respectively). We
592 highlight this issue to draw attention to some of the problems inherent in modelling TE solubility and
593 its impact on the chemistry and biogeochemistry of the upper ocean.

594 Given that the different leaching approaches access different fractions of aerosol TEs that can dissolve
595 from aerosols at different rates (e.g. TEs loosely bound to surfaces and TEs that are associated with
596 less reactive phases) (e.g. Kocak et al., 2007; Mackey et al., 2015), we need to conduct experiments
597 that elucidate the relationship between the soluble and bioavailable fractions. In the meantime, we
598 suggest that the 25 % acetic acid leach might be better to estimate the bioavailable fraction given that
599 Fe (and perhaps other TEs) associated with lithogenic particles are directly available to micro-
600 organisms in productive regions and regions with high dust inputs (Rubin et al., 2011) and that aerosol
601 particles can be processed by zooplankton (Schmidt et al., 2016).

602

603 **4. Conclusions**

604 Aerosol TE solubility is usually determined using operationally-defined methods, while
605 biogeochemical models require robust relationships between two or more parameters that can be used
606 to predict TE solubility in order to constrain the bioavailable fraction of aerosol TEs. In this study, we
607 used a two-stage leach (UHP water followed by 25 % acetic acid with hydroxylamine hydrochloride)
608 to investigate the fractional solubility of a suite of trace elements (Al, Ti, Mn, Fe, Co, Ni, Cu, Zn, Cd,
609 Pb) from aerosols collected in the North Atlantic during three GEOTRACES campaigns (GA03-2010,
610 GA03-2011 and GA01). Five regions were identified based on air mass back trajectory (AMBT)
611 simulations; i) North Africa, ii) Europe, iii) North America, iv) High Latitude, and v) Marine.
612 However, the AMBTs were not able to sufficiently discriminate aerosol sources within these regions.
613 Of these five categories, the North African aerosols were the most homogeneous in terms of their
614 fractional solubility and elemental ratios. In contrast, samples from the most remote locations, the
615 Marine and High Latitude aerosols, had the most spread in their fractional solubility and elemental
616 ratios. Elemental ratios were discussed rather than enrichment factors normalised to UCC composition
617 since earlier work highlighted that the UCC ratios are not representative of the North African mineral
618 dust end-member, which dominates aerosol supply in much of the study area.

619 We observed an inverse relationship between the fractional solubility of Al, Ti, Fe, Ni, Cu and Pb and
620 aerosol loading for all leach media (UHP water, filtered seawater, and 25 % acetic acid with
621 hydroxylamine hydrochloride). However, Mn, Zn and Cd fractional solubility appears to be
622 independent of atmospheric loading. For Co, the inverse relationship between UHP water solubility

623 and loading was not observed when using the 25 % acetic acid leach, most likely because Co may be
624 associated with the Mn and Fe oxides that are easily reduced using the 25 % acetic acid leach. Further
625 work is required to assess exactly which fraction is accessed by the various leach protocols in order to
626 understand links between the soluble and bioavailable fractions.

627

628 **Data availability**

629 Data is available at BCO-DMO (GA03; www.bco-dmo.org) and LEFE-CYBER (GA01;
630 (www.obsvlfr.fr/proof/php/GEOVIDE/GEOVIDE.php), and on request from the lead author.

631 **Acknowledgements**

632 Many thanks to the captains and crews of the RV Knorr (GA03-2010 and 2011) and NO Pourquoi
633 Pas? (GA01), the chief scientists (GA03 = Bob Anderson, Ed Boyle, Greg Cutter; GA01 = Geraldine
634 Sarthou and Pascale Lherminier), Alex Baker for the loan of the aerosol sampler used on GA01, and
635 Alina Ebling Petroc Shelley, Alex Landing and Sarah Huff for their help with sample processing and
636 analysis. This work was supported by grants to WML (NSF-OCE 0752832, 0929919 and 1132766),
637 and GS (ANR-13-B506-0014 and ANR-12-PDOC-0025-01). RUS was supported by a LabexMER
638 International Postdoctoral Fellowship and CG29 Postdoctoral Fellowship. A portion of this work was
639 performed at the National High Magnetic Field Laboratory, which is supported by National Science
640 Foundation Cooperative Agreement No. DMR-1157490 and the State of Florida. The aerosol
641 digestions for GA01 were undertaken in the geochemistry clean room at Ifremer (Centre de Bretagne).
642 Trace element determination for GA01 was conducted at the Pôle de Spectrométrie Océan at the
643 Institut Universitaire Européen de la Mer with the support and guidance of Claire Bollinger and
644 Marie-Laure Rouget. Finally, we thank Karine Desbeoufs and an anonymous reviewer for their
645 critiques that have contributed to the improvement of this manuscript.

646

647 **References**

- 648 Achterberg, E. P., Moore, C.M., Henson, S. A., Steigenberger, S., Stohl, A., Eckhardt, S., Avendano,
649 LC., Cassidy, M., Hembury, D., Klar, J.K., Lucas, M.I., Macey, A.I., Marsay, C.M., and, Ryan-
650 Keogh, T.J.: Natural iron fertilization by the Eyjafjallajökull volcanic eruption, *Geophys. Res. Lett.*,
651 40, 921-926, <http://doi.org/10.1002/grl.50221>, 2013.
- 652 Adams, A. M., Prospero, J.M., and Zhang, C.: CALIPSO-Derived Three-Dimensional Structure of
653 Aerosol over the Atlantic Basin and Adjacent Continents, *Journal of Climate*, 25, 6862-6879,
654 <http://doi.org/10.1175/JCLI-D-11-00672.1>, 2012.
- 655 Aguilar-Islas, A. M., Wu, J., Rember, R., Johansen, A.M. and Shank, L. M.: Dissolution of aerosol-
656 derived iron in seawater: Leach solution chemistry, aerosol type, and colloidal iron fraction, *Marine*
657 *Chemistry*, 120, 25-33., 2010.

658 Arnalds, O.: Soils of Iceland, *Jökull*, 58, 409-421, 2004.

659 Baker, A. R., Adams, C., Bell, T.G., Jickells, T.D., and Ganzeveld, L.: Estimation of atmospheric
660 nutrient inputs to the Atlantic Ocean from 50N to 50S based on large-scale field sampling: Iron and
661 other dust-associated elements, *Global Biogeochem. Cycles*, 27, 755-767,
662 <http://doi.org/10.1002/gbc.20062>, 2013, 2013.

663 Baker, A. R., and Croot, P. L.: Atmospheric and marine controls on aerosol iron solubility in
664 seawater., *Marine Chemistry*., 120, 4-13, 2010.

665 Baker, A. R., and Jickells, T.D.: Mineral particle size as a control on aerosol iron solubility., *Geophys.*
666 *Res. Lett.*, 33, <http://doi.org/10.1029/2006GL026557>, 2006.

667 Baker, A. R., and Jickells, T.D.: Atmospheric deposition of soluble trace elements along the Atlantic
668 Meridional Transect (AMT), *Progress in Oceanography*, 158, 41-51, 10.1016/j.pocean.2016.10.002,
669 2017.

670 Baker, A. R., Jickells, T. D., Biswas, K. F., Weston, K., and French, M.: Nutrients in atmospheric
671 aerosol particles along the Atlantic Meridional Transect, *Deep Sea Research Part II: Topical Studies in*
672 *Oceanography*, 53, 1706-1719, 2006a.

673 Baker, A. R., Jickells, T. D., Witt, M., and Linge, K. L.: Trends in the solubility of iron, aluminium,
674 manganese and phosphorus in aerosol collected over the Atlantic Ocean, *Marine Chemistry*, 98, 43-58,
675 2006b.

676 Baker, A. R., Landing, W.M., Bucciarelli, E., Cheize, M., Fietz, S., Hayes, C.T., Kadko, D., Morton,
677 P.L., Rogan, N., Sarthou, G., Shelley, R.U., Shi, Z., Shiller, A., and, van Hulst, M.M.P.: Trace
678 element and isotope deposition across the air–sea interface: progress and research needs, *Philosophical*
679 *Transactions of the Royal Society A: Mathematical, Physical and Engineering Sciences*, 374,
680 <http://doi.org/10.1098/rsta.2016.0190>, 2016.

681 Baratoux, D., Mangold, N., Arnalds, O., Bardintzeff, J.-M., Platevoët, B., Grégoire, M., and Pinet, P.:
682 Volcanic sands of Iceland - Diverse origins of aeolian sand deposits revealed at Dyngjúsandur and
683 Lambhraun, *Earth Surf. Process. Landforms*, 36, 1789-1808, 10.1002/esp.2201, 2011.

684 Ben-Ami, Y., Koren, I., Rudich, Y., Artaxo, P., Martin, S.T., and Andreae, M.O.: Transport of North
685 African dust from the Bodele depression to the Amazon Basin: a case study, *Atmos. Chem. Phys.*, 10,
686 7533-7544, <http://doi.org/10.5194/acp-10-7533-2010>, 2010.

687 Berger, J. M., Lippiatt, S.M., Lawrence, M.G., and Bruland, K.W.: Application of a chemical leach
688 technique for estimating labile particulate aluminum, iron, and manganese in the Columbia River
689 plume and coastal waters off Oregon and Washington., *Journal of Geophysical Research*, 113,
690 <http://doi.org/10.1029/2007JC004703>, 2008.

691 Bridgestock, L., Rehkämper, M., van de Flierdt, T., Murphy, K., Khondoker, R., Baker, A. R., Chance,
692 R., Strekopytov, S., Humphreys-Williams, E., and Achterberg E.P.: The Cd isotope composition of
693 atmospheric aerosols from the Tropical Atlantic Ocean, *Geophys. Res. Lett.*, 44, 2932-2940,
694 <http://doi.org/10.1002/2017GL072748>, 2017.

695 Buck, C. S., Landing, W.M., and Resing, J.: Pacific Ocean aerosols: Deposition and solubility of iron,
696 aluminum, and other trace elements, *Marine Chemistry*, 157, 117-130,
697 <http://dx.doi.org/10.1016/j.marchem.2013.09.005>, 2013.

- 698 Buck, C. S., Landing, W.M., Resing, J. A., Lebon, G. T.: Aerosol iron and aluminum solubility in the
699 northwest Pacific Ocean: Results from the 2002 IOC cruise, *Geochemistry, Geophysics, Geosystems.*,
700 7, <http://doi.org/10.1029/2005GC000977>, 2006.
- 701 Buck, C. S., Landing, W.M., Resing, J.A. and Measures, C.I.: The solubility and deposition of aerosol
702 Fe and other trace elements in the North Atlantic Ocean: Observations from the A16N CLIVAR/CO₂
703 repeat hydrography section., *Marine Chemistry.*, 120, 57-70, 2010.
- 704 Bullard, J. E., Baddock, M., Bradwell, T., Crusius, J., Darlington, E., Gaiero, D., Gassó, S.,
705 Gisladottir, G., Hodgkins, R., McCulloch, R., McKenna-Neuman, C., Mockford, T., Stewart, H., and,
706 Thorsteinsson, T.: High-latitude dust in the Earth system, *Reviews of Geophysics*, 54, 447-485,
707 <http://doi.org/10.1002/2016RG000518>, 2016.
- 708 Cheize, M., Sarthou, G., Croot, P., Bucciarelli, E., Baudoux, A.-C., and Baker, A.: Iron organic
709 speciation determination in rainwater using cathodic stripping voltammetry, *Analytica Chimica Acta*,
710 726, 45-54, 2012.
- 711 Chiapello, I., Bergametti, G., Chatenet, B., Bousquet, P., Dulac, F., and Soares, E. S.: Origins of
712 African dust transported over the northeastern tropical Atlantic, *Journal of Geophysical Research:*
713 *Atmospheres*, 102, 13701-13709, [10.1029/97jd00259](http://doi.org/10.1029/97jd00259), 1997.
- 714 Chueinta, W., Hopke, P. K., and Paatero, P.: Investigation of sources of atmospheric aerosol at urban
715 and suburban residential areas in Thailand by positive matrix factorization, *Atmospheric Environment*,
716 34, 3319-3329, [http://dx.doi.org/10.1016/S1352-2310\(99\)00433-1](http://dx.doi.org/10.1016/S1352-2310(99)00433-1), 2000.
- 717 Conway, T. M., and John, S.G.: Quantification of dissolved iron sources to the North Atlantic Ocean,
718 *Nature*, 511, 212-215, <http://doi.org/10.1038/nature13482>. 2014.
- 719 Conway, T.M., Shelley, R.U., Aguilar-Islas, A.M., Landing, W.M., Mahowald, N.M., and John, S.G.:
720 Iron isotopes reveal an important anthropogenic aerosol iron flux to the North Atlantic. Submitted to:
721 *Nature Communications*.
- 722 de Leeuw, G., Guieu, C., Arneth, A., Bellouin, N., Bopp, L., Boyd, P.W., Denier van der Gon, H.A.C.,
723 Desboeufs, K.V., Dulac, F., Facchini, M.C., Gantt, B., Langmann, B., Mahowald, N.M., Maranon, E.,
724 O'Dowd, C., Olgun, N., Pulido-Villena, E., Rinaldi, M., Stephanou, E.G., and Wagener, T. : Ocean-
725 atmosphere interactions of particles, in: *Ocean-atmosphere interactions of gases and particles*, edited
726 by: Liss, P. S., and Johnson, M.T., Springer-Verlag, Berlin, 171-245, 2014.
- 727 Desboeufs, K. V., Sofikitis, A., Losno, R., Colin, J. L. and Ausset, P.: Dissolution and solubility of
728 trace metals from natural and anthropogenic aerosol particulate matter., *Chemosphere*, 58, 195-203.,
729 2005.
- 730 Doherty, O. M., Riemer, N., and Hameed, S.: Role of the convergence zone over West Africa in
731 controlling Saharan mineral dust load and transport in the boreal summer, *Tellus B*, 66,
732 <http://doi.org/10.3402/tellusb.v66.23191>, 2014.
- 733 Fishwick, M. P., Sedwick, P.N., Lohan, M.C., Worsfold, P.J., Buck, K.N., Church, T.M., and Ussher,
734 S.J.: The impact of changing surface ocean conditions on the dissolution of aerosol iron, *Global*
735 *Biogeochem. Cycles*, 28, 1235-1250, <http://doi.org/10.1002/2014GB004921>, 2014.

- 736 Gelado-Caballero, M. D., López-García, P., Prieto, S., Patey, M.D., Collado, C., Hernández-Brito, J.J.:
737 Long-term aerosol measurements in Gran Canaria, Canary Islands: Particle concentration, sources and
738 elemental composition, *Journal of Geophysical Research: Atmospheres*, 117, D03304,
739 <http://doi.org/10.1029/2011jd016646>, 2012.
- 740 GEOTRACES Planning Group, GEOTRACES Science Plan. Baltimore, Maryland:
741 Scientific Committee on Oceanic Research, <http://www.geotraces.org/science/science-plan>, 2006.
- 742 Gledhill, M., and Buck, K. N.: The organic complexation of iron in the marine environment: a review,
743 *Frontiers in Microbiology*, <https://doi.org/10.3389/fmicb.2012.00069>, 2012.
- 744 Hatta, M., Measures, C. I., Wu, J., Roshan, S., Fitzsimmons, J. N., Sedwick, P., and, and Morton, P.:
745 An overview of dissolved Fe and Mn Distributions during the 2010–2011 U.S. GEOTRACES north
746 Atlantic Cruises: GEOTRACES GA03, Deep Sea Research Part II: Topical Studies in Oceanography,
747 <http://dx.doi.org/10.1016/j.dsr2.2014.07.005>, 2015.
- 748 Helmers, E., and Schrems, O.: Wet deposition of metals to the tropical North and the South Atlantic
749 Ocean, *Atmospheric Environment*, 29, 2475-2484, 1995.
- 750 Jickells, T. D., Baker, A. R., and Chance, R.: Atmospheric transport of trace elements and nutrients to
751 the oceans, *Philosophical Transactions of the Royal Society A: Mathematical, Physical and*
752 *Engineering Sciences*, 374, <http://doi.org/10.1098/rsta.2015.0286>, 2016.
- 753 Jickells, T. D., An, Z.S., Andersen, K.K., Baker, A.R., Bergametti, G., Brooks, N., Cao, J.J., Boyd,
754 P.W., Duce, R.A., Hunter, K.A., Kawahata, H., Kubilay, N., laRoche, J., Liss, P.J., Mahowald, N.,
755 Prospero, J.M., Ridgwell, A.J., Tegen, I., and Torres, R.: Global iron connections between desert dust,
756 ocean biogeochemistry and climate., *Science*, 308, 67-71, 2005.
- 757 Johansen, A., Siefert, R.L., Hoffmann, M.R.: Chemical composition of aerosols collected over the
758 tropical North Atlantic Ocean, *Journal of Geophysical Research*, 105, 15277-15312, 2000.
- 759 Johnson, B. T., Osborne, S.R., Haywood, J.M., and Harrison, M.A.J.: Aircraft measurements of
760 biomass burning aerosol over West Africa during DABEX, *J. Geophys. Res.*, 113,
761 [10.1029/2007JD009451](http://doi.org/10.1029/2007JD009451), 2008.
- 762 Kim, G., Alleman, L.Y., and Church, T.M.: Atmospheric depositional fluxes of trace elements, 210Pb,
763 and 7Be to the Sargasso Sea, *Global Biogeochemical Cycles*, 13, <http://doi.org/10.1029/1999gb900071>, 1999.
- 765 Knippertz, P., Coe, H., Chiu, J. C., Evans, M.J., Fink, A.H., Kalthoff, N., Lioussé, C., Mari, C.,
766 Allan, R.P., Brooks, B., Danour, S., Flamant, C., Jegede, O.O., Lohou, F., and, Marsham, J.H.: The
767 DACCIWA Project: Dynamics–Aerosol–Chemistry–Cloud Interactions in West Africa, *Bulletin of the*
768 *American Meteorological Society*, 96, 1451-1460, [10.1175/BAMS-D-14-00108.1](http://doi.org/10.1175/BAMS-D-14-00108.1), 2015.
- 769 Koçak, M., Kubilay, N., Herut, B., and Nimmo, M.: Trace Metal Solid State Speciation in Aerosols of
770 the Northern Levantine Basin, East Mediterranean, *Journal of Atmospheric Chemistry*, 56, 239-257,
771 <http://doi.org/10.1007/s10874-006-9053-7>, 2007.
- 772 Lafon, S., Sokolik, I. N., Rajot, J. L., Caqueneau, S. and Gaudichet, A.: Characterization of iron oxides
773 in mineral dust aerosols: Implications for light absorption, *J. Geophys. Res.*, 111,
774 [10.1029/2005JD007016](http://doi.org/10.1029/2005JD007016), 2006.

775 Laing, J. R., Hopke, P.K., Hopke, E.F., Husain, L., Dutkiewicz, V.A., Paatero, J., and Viisanen, Y.:
776 Positive Matrix Factorization of 47 Years of Particle Measurements in Finnish Arctic, *Aerosol and Air*
777 *Quality Research*, 15, 188-207, <http://doi.org/10.4209/aaqr.2014.04.0084>, 2015.

778 Landing, W.M., and Shelley, R.U.: Particle size effects on aerosol iron solubility from the U.S.
779 GEOTRACES North Atlantic Zonal Transect (2010, 2011), ASLO 2013 Aquatic Sciences Meeting,
780 2013.

781 Longhurst, A.: *Ecological Geography of the Sea.*, Academic Press., San Diego, 1998.

782 Longo, A. F., Feng, Y., Lai, B., Landing, W.M., Shelley, R.U., Nenes, A., Mihalopoulos, N., Violaki,
783 K., and, Ingall, E.D.: Influence of Atmospheric Processes on the Solubility and Composition of Iron in
784 Saharan Dust, *Environmental Science & Technology*, 50, 6912-6920,
785 <http://doi.org/10.1021/acs.est.6b02605>, 2016.

786 Mackey, K. R. M., Chien, C.-T., Post, A.F., Saito, M.A., and Paytan, A.: Rapid and gradual modes of
787 aerosol trace metal dissolution in seawater, *Frontiers in Microbiology*, 5, 1-11,
788 <http://doi.org/10.3389/fmicb.2014.00794>, 2015.

789 Maring, H., Settle, D.M., Buat-Ménard, P., Dulac, F., and, Patterson, C.C.: Stable lead isotopes tracers
790 of air mass trajectories in the Mediterranean region, *Nature*, 300, 154-156, 1987.

791 Marticorena, B., Chatenet, B., Rajot, J. L., Traoré, S., Coulibaly, M., Diallo, A., Koné, I., Maman, A.,
792 Ndiaye, T., and Zakou, A.: Temporal variability of mineral dust concentrations over West Africa:
793 analyses of a pluriannual monitoring from the AMMA Sahelian Dust Transect, *Atmos. Chem. Phys.*,
794 10, 8899-8915, [10.5194/acp-10-8899-2010](https://doi.org/10.5194/acp-10-8899-2010), 2010.

795 McConnell, C. L., Highwood, E.J., Coe, H., Formenti, P., Anderson, B., Osborne, S., Nava, S.,
796 Desboeufs, K., Chen, G., and Harrison, M.A.J.: Seasonal variations of the physical and optical
797 characteristics of Saharan dust: Results from the Dust Outflow and Deposition to the Ocean (DODO)
798 experiment, *Journal of Geophysical Research: Atmospheres*, 113, D14S05, [10.1029/2007jd009606](https://doi.org/10.1029/2007jd009606),
799 2008.

800 Measures, C.I., and Brown E.T.: Estimating dust input to the Atlantic Ocean using surface water Al
801 concentrations, in, *The Impact of desert dust across the Mediterranean*, edited by S. Guerzoni and R.
802 Chester, pp.301-311, Kluwer: Dordrecht, 1996.

803 Menzel-Barraqueta, J.-L., Schlosser, C., Planquette, H., Gourain, A., Cheize, M., Boutorh, J., Shelley,
804 R., Pereira Contreira, L., Gledhill, M., Hopwood, M.J., Lherminier, P., Sarthou, G. and Achterberg,
805 E.P. Aluminium in the North Atlantic Ocean and the Labrador Sea (GEOTRACES GA01 section):
806 roles of continental inputs and biogenic particle removal. *Biogeosciences Discuss.*,
807 <https://doi.org/10.5194/bg-2018-39>, this issue.

808 Morton, P. L., Landing, W.M., Hsu, S.-C., Milne, A., Aguilar-Islas, A.M., Baker, A.R., Bowie, A.R.,
809 Buck, C.S., Gao, Y., Gichuki, S., Hastings, M.G., Hatta, M., Johansen, A. M., Losno, R., Mead, C.,
810 Patey, M.D., Swarr, G., Vandermark, A., Zamora, L.M.: Methods for the sampling and analysis of
811 marine aerosols: results from the 2008 GEOTRACES aerosol intercalibration experiment, *Limnology*
812 *and Oceanography: Methods*, 11, 62-78, 2013.

813 Oladottir, B. A., Sigmarsson, O., Larsen, G., and Devidal, J.L.: Provenance of basaltic tephra from
814 Vatnajökull subglacial volcanos, iceland, as determined by major- and trace-element analyses, *The*
815 *Holocene*, 21, 1037-1048, [10.1177/0959683611400456](https://doi.org/10.1177/0959683611400456), 2011.

- 816 Patey, M. D., Achterberg, E.P., Rijkenberg, M.J., and Pearce, R.: Aerosol time-series measurements
817 over the tropical Northeast Atlantic Ocean: Dust sources, elemental, composition and mineralogy,
818 *Marine Chemistry*, 174, 103-119, <http://dx.doi.org/10.1016/j.marchem.2015.06.004>, 2015.
- 819 Petzold, A., Rasp, K., Weinzierl, B., Esselborn, M., Hamburger, T., Dörnbrack, A., Kandler, K.,
820 Schütz, L., Knippertz, P., Fiebig, M., and Virkkula, A.: Saharan dust absorption and refractive index
821 from aircraft-based observations during SAMUM 2006, *Tellus B*, 61, 118-130, [10.1111/j.1600-0889.2008.00383.x](https://doi.org/10.1111/j.1600-0889.2008.00383.x), 2009.
- 823 Planquette, H., Gourain, A., Cheize, M., Menzel Barraqueta, J.L., Boutorh, J., Shelley, R., Pereira
824 Contreira, L., Lacan, F., Lherminier, P. and Sarthou, G. Particulate trace elements in the North
825 Atlantic along the GEOVIDE section (GEOTRACES GA01), ASLO 2016 Ocean Sciences Meeting,
826 2016.
- 827 Powell, C. F., Baker, A.R., Jickells, T.D., Bange, H.W., Chance, R.J., Yodle, C.: Estimation of the
828 atmospheric flux of nutrients and trace metals to the eastern tropical North Atlantic Ocean, *Journal of*
829 *the Atmospheric Sciences*, 4029-4045, <http://doi.org/10.1175/JAS-D-15-0011.1>, 2015.
- 830 Prospero, J. M., Bullard, J.E., and Hodgkins, R.: High-Latitude Dust Over the North Atlantic: Inputs
831 from Icelandic Proglacial Dust Storms, *Science*, 335, 1078-1082,
832 <http://doi.org/10.1126/science.1217447>, 2012.
- 833 Prospero, J. M., Ginoux, P., Torres, O., Nicholson, S.E. and Thomas, T.E.: Environmental
834 characterization of global sources of atmospheric dust identified with the Nimbus 7 Total Ozone
835 Mapping Spectrometer (TOMS) absorbing aerosol product., *Reviews of Geophysics.*, 40,
836 [10.1029/2000RG000095](https://doi.org/10.1029/2000RG000095), 2002.
- 837 Prospero, J. M., Glaccum, R.A. and Nees, R.T.: Atmospheric transport of soil dust from Africa to
838 South America., *Nature.*, 289, 570-572., 570-572., 1981.
- 839 R Core Team: R: A Language and Environmental for Statistical Computing. [https://www.R-](https://www.R-project.org/)
840 [project.org.](https://www.R-project.org/), 2016.
- 841 Rolph, G.D., Real-time Environmental Applications and Display sYstem (READY) Website
842 (<http://ready.arl.noaa.gov>). NOAA Air Resources Laboratory, Silver Spring, MD, 2017. Rubin, M.,
843 Berman-Frank, I., and Shaked, Y.: Dust- and mineral-iron utilization by the marine dinitrogen-fixer
844 *Trichodesmium*, *Nature Geosci*, 4, 529-534, 2011.
- 845 Rudnick, R. L., and Gao, S.: Composition of the continental crust, in: *Treatise on Geochemistry*,
846 edited by: Holland, H. D., and Turekian, K.K., Elsevier, Oxford, 1-64, <http://dx.doi.org/10.1016/B0-08-043751-6/03016-42003>.
- 848 Rue, E. L., and Bruland, K. W. : Complexation of iron (III) by natural organic ligands in the Central
849 North Pacific as determined by a new competitive ligand equilibrium/ adsorptive cathodic stripping
850 voltammetric method, *Marine Chemistry*, 50, 117-138, 1995.
- 851 Sarthou, G., Baker, A.R., Blain, S., Achterberg, E.P., Boye, M., Bowie, A.R., Croot, P., Laan, P., de
852 Baar, H.J. W., Jickells, T.D. and Worsfold, P.J.: Atmospheric iron deposition and sea-surface
853 dissolved iron concentrations in the eastern Atlantic Ocean., *Deep Sea Research Part I: Oceanographic*
854 *Research Papers.*, 50, 1339-1352., 2003.
- 855 Scheuven, D., Schütz, L., Kandler, K., Ebert, M., and Weinbruch, S.: Bulk composition of northern
856 African dust and its source sediments — A compilation, *Earth-Science Reviews*, 116, 170-194,
857 <http://dx.doi.org/10.1016/j.earscirev.2012.08.005>, 2013.

- 858 Schmidt, K., Schlosser, C., Atkinson, A., Fielding, S., Venables, H.J., Waluda, C.M., and Achterberg,
859 E.P.: Zooplankton gut passage mobilizes lithogenic iron for ocean productivity, *Current Biology*, 26,
860 2667-2673, <https://doi.org/10.1016/j.cub.2016.07.058>, 2016.
- 861 Sedwick, P. N., Sholkovitz, E.R. and Church, T.M.: Impact of anthropogenic combustion emissions on
862 the fractional solubility of aerosol iron: evidence from the Sargasso Sea., *Geochemistry, Geophysics,*
863 *Geosystems.*, 8, <http://doi.org/10.1029/2007GC001586>, 2007.
- 864 Sippula, O., Stengel, B., Sklorz, M., Streibel, T., Rabe, R., Orasche, J., Lintelmann, J., Michalke, B.,
865 Abbaszade, G., Radischat, C., Gröger, T., Schnelle-Kreis, J., Harndorf, H., and Zimmermann, R.:
866 Particle Emissions from a Marine Engine: Chemical Composition and Aromatic Emission Profiles
867 under Various Operating Conditions, *Environmental Science & Technology*, 48, 11721-11729,
868 [10.1021/es502484z](https://doi.org/10.1021/es502484z), 2014.
- 869 Shaked, Y., and Lis, H.: Dissassembling iron availability to phytoplankton, *Frontiers in Microbiology*,
870 3, <http://doi.org/10.3389/fmicb.2012.00123>, 2012.
- 871 Shelley, R. U., Morton, P.L. and Landing, W.M.: Elemental ratios and enrichment factors in aerosols
872 from the US-GEOTRACES North Atlantic transects, *Deep Sea Research Part II: Topical Studies in*
873 *Oceanography*, 116, 262-272, <http://dx.doi.org/10.1016/j.dsr2.2014.12.005>, 2015.
- 874 Shelley, R. U., Roca-Martí, M., Castrillejo, M., Sanial, V., Masqué, P., Landing, W.M., van Beek, P.,
875 Planquette, H., and Sarthou, G.: Quantification of trace element atmospheric deposition fluxes to the
876 Atlantic Ocean (> 40°N; GEOVIDE, GEOTRACES GA01) during spring 2014, *Deep Sea Research*
877 *Part I: Oceanographic Research Papers*, 119, 34-49, <http://doi.org/10.1016/j.dsr.2016.11.010>, 2017.
- 878 Sholkovitz, E., R., Sedwick, P.N. and Church, T.M.: Influence of anthropogenic combustion emissions
879 on the deposition of soluble aerosol iron to the ocean: Empirical estimates for island sites in the North
880 Atlantic., *Geochimica et Cosmochimica Acta.*, 73, 3981-4003., 2009.
- 881 Sholkovitz, E., R., Sedwick, P.N., Church, T.M., Baker, A.R., and Powell, C.F.: Fractional solubility
882 of aerosol iron: Synthesis of a global-scale data set, *Geochimica et Cosmochimica Acta*, 89, 173-189,
883 2012.
- 884 Skonieczny, C., Bory, A. Bout-Roumazeilles, V., Abouchami, W., Galer, S. J. G., Crosta, X. Stuut,
885 J.-B., I. Meyer, Chiapello, I., Podvin, T., Chatenet, B., Diallo, A., and Ndiaye, T.: The 7–13 March
886 2006 major Saharan outbreak: Multiproxy characterization of mineral dust deposited on the West
887 African margin, *Journal of Geophysical Research*, 116, <http://doi.org/10.1029/2011JD016173>, 2011.
- 888 Stein, A.F., Draxler, R.R, Rolph, G.D., Stunder, B.J.B., Cohen, M.D., and Ngan, F.: NOAA's
889 HYSPLIT atmospheric transport and dispersion modeling system, *Bull. Amer. Meteor. Soc.*, 96, 2059-
890 2077, <http://doi.org/10.1175/BAMS-D-14-00110.1>, 2015.
- 891 Tonnard, M., Planquette, H., Bowie, A.R., van der Merwe, P., Gallinari, M., Desprez de Gésincourt,
892 F., Germain, Y., Gourain, A., Benetti, M., Reverdin, G., Treguer, P., Boutorh, J., Cheize, M., Menzel-
893 Barraqueta, J.L., Pereira-Contreira, L., Shelley, R., Lherminier, P., and Sarthou, G. Dissolved iron in
894 the North Atlantic Ocean and Labrador Sea along the GEOVIDE section (GEOTRACES section
895 GA01), Submitted to *Biogeosciences Discuss.*, this issue.
- 896 Ussher, S. J., Achterberg, E.P., Powell, C., Baker, A.R., Jickells, T.D., Torres, R., and Worsfold, P.J.:
897 Impact of atmospheric deposition on the contrasting iron biogeochemistry of the North and South
898 Atlantic Ocean, *Global Biogeochemical Cycles*, 27, 1096-1107, <http://doi.org/10.1002/gbc.20056>,
899 2013.

- 900 Weber, R. J., Guo, H., Russell, A.G., and Nenes, A.: High aerosol acidity despite declining
901 atmospheric sulfate concentrations over the past 15 years, *Nature Geosci*, 9, 282-285,
902 <http://doi.org/10.1038/ngeo2665>
- 903 Wozniak, A. S., Shelley, R.U., McElhenie, S.D., Landing, W.M., and Hatcher, P.G.: Aerosol water
904 soluble organic matter characteristics over the North Atlantic Ocean: Implications for iron-binding
905 ligands and iron solubility, *Marine Chemistry*, 173, 162-172,
906 <http://dx.doi.org/10.1016/j.marchem.2014.11.002>, 2015.
- 907 Wozniak, A. S., Shelley, R.U., Sleighter, R.L., Abdulla, H.A.N., Morton, P.L., Landing, W.M., and
908 Hatcher, P.G.: Relationships among aerosol water soluble organic matter, iron and aluminum in
909 European, North African, and Marine air masses from the 2010 US GEOTRACES cruise, *Marine
910 Chemistry*, 154, 24-33, <http://dx.doi.org/10.1016/j.marchem.2013.04.011>, 2013.
- 911 Wozniak, A. S., Willoughby, A. S., Gurganus, S. C., and Hatcher, P. G.: Distinguishing molecular
912 characteristics of aerosol water soluble organic matter from the 2011 trans-North Atlantic US
913 GEOTRACES cruise, *Atmos. Chem. Phys.*, 14, 8419-8434, 10.5194/acp-14-8419-2014, 2014.
- 914 Zurbrick, C., Boyle, E., Kayser, R., Reuer, M., Wu, J., Planquette, H., Shelley, R., Boutorh, J., Cheize,
915 M., Contreira, L., Menzel, J.L. and Sarthou, G. Dissolved Pb and Pb isotopes in the North Atlantic
916 from the GEOVIDE transect (GEOTRACES GA-01) and heir decadal evolution. *Biogeosciences
917 Discuss*, <https://doi.org/10.5194/bg-2018-29>.

918

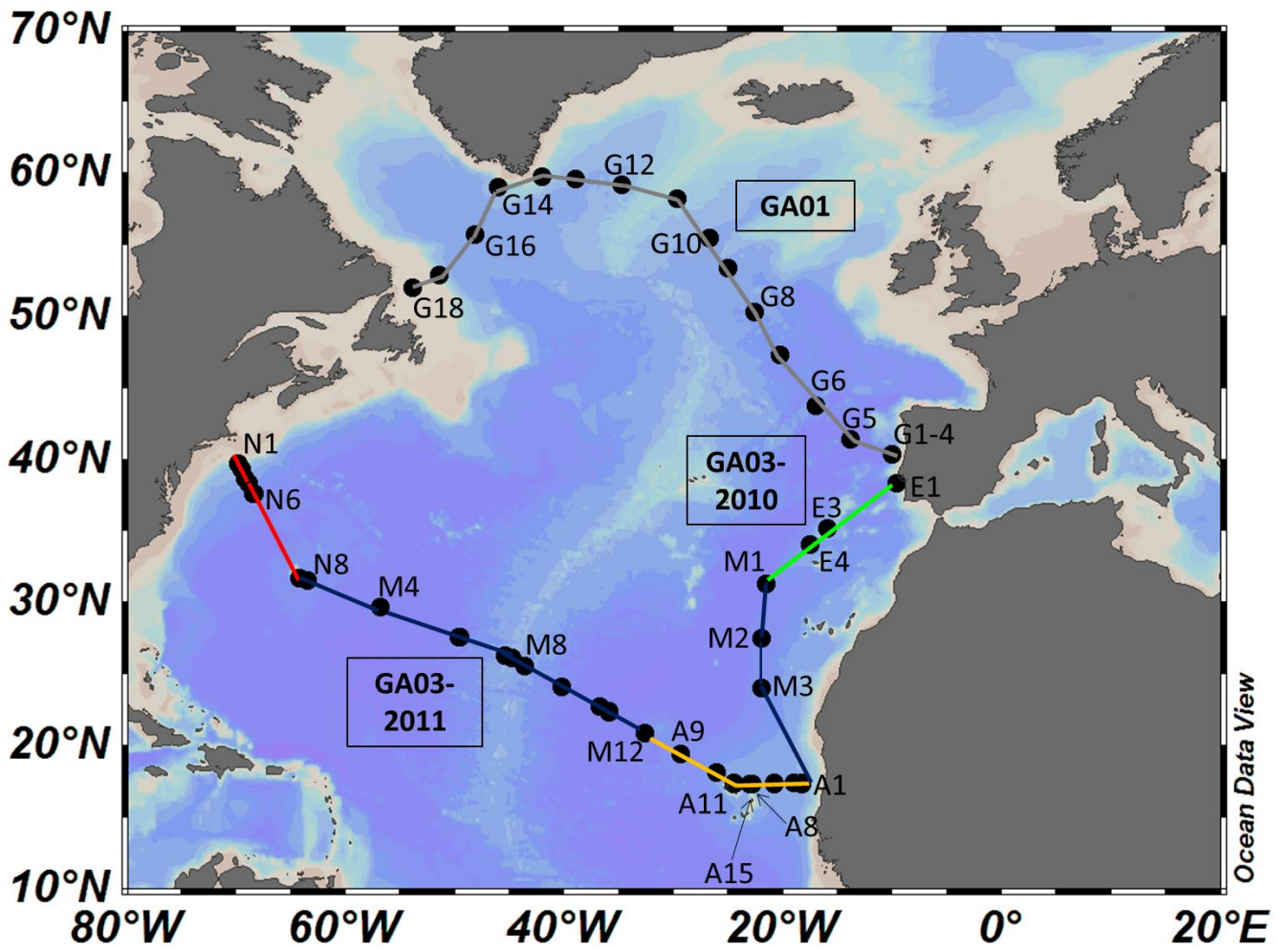
919

920

921

922

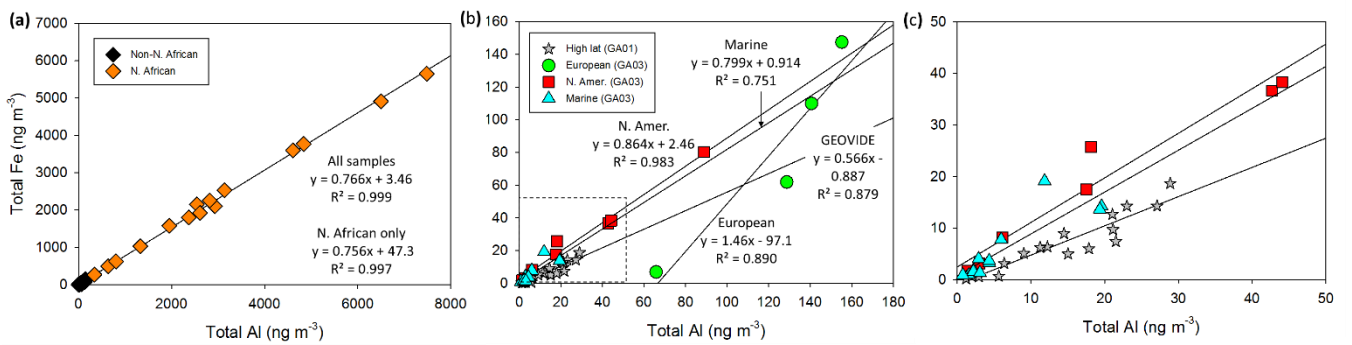
923



924

Figure 1

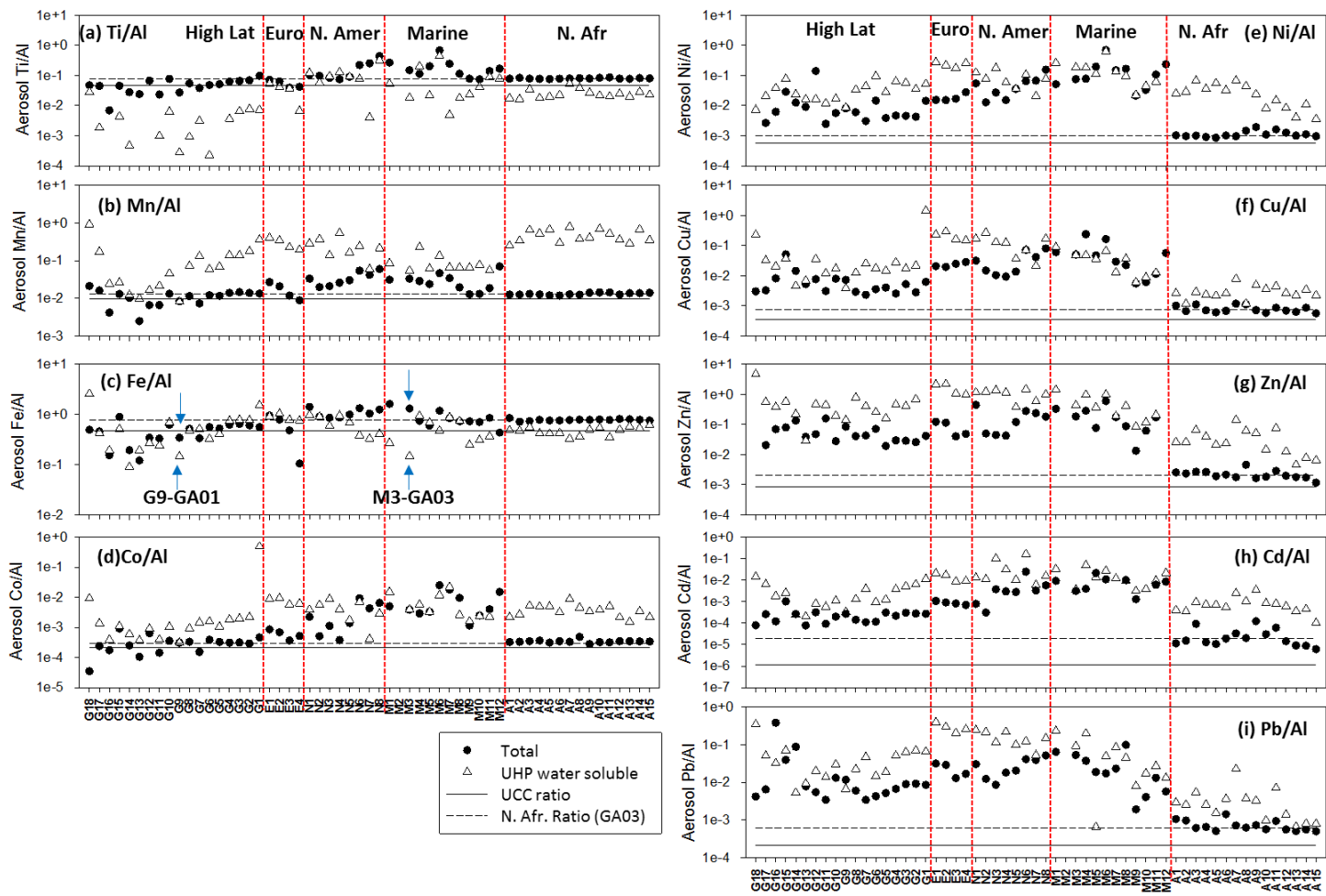
925
926
927
928
929
930



931

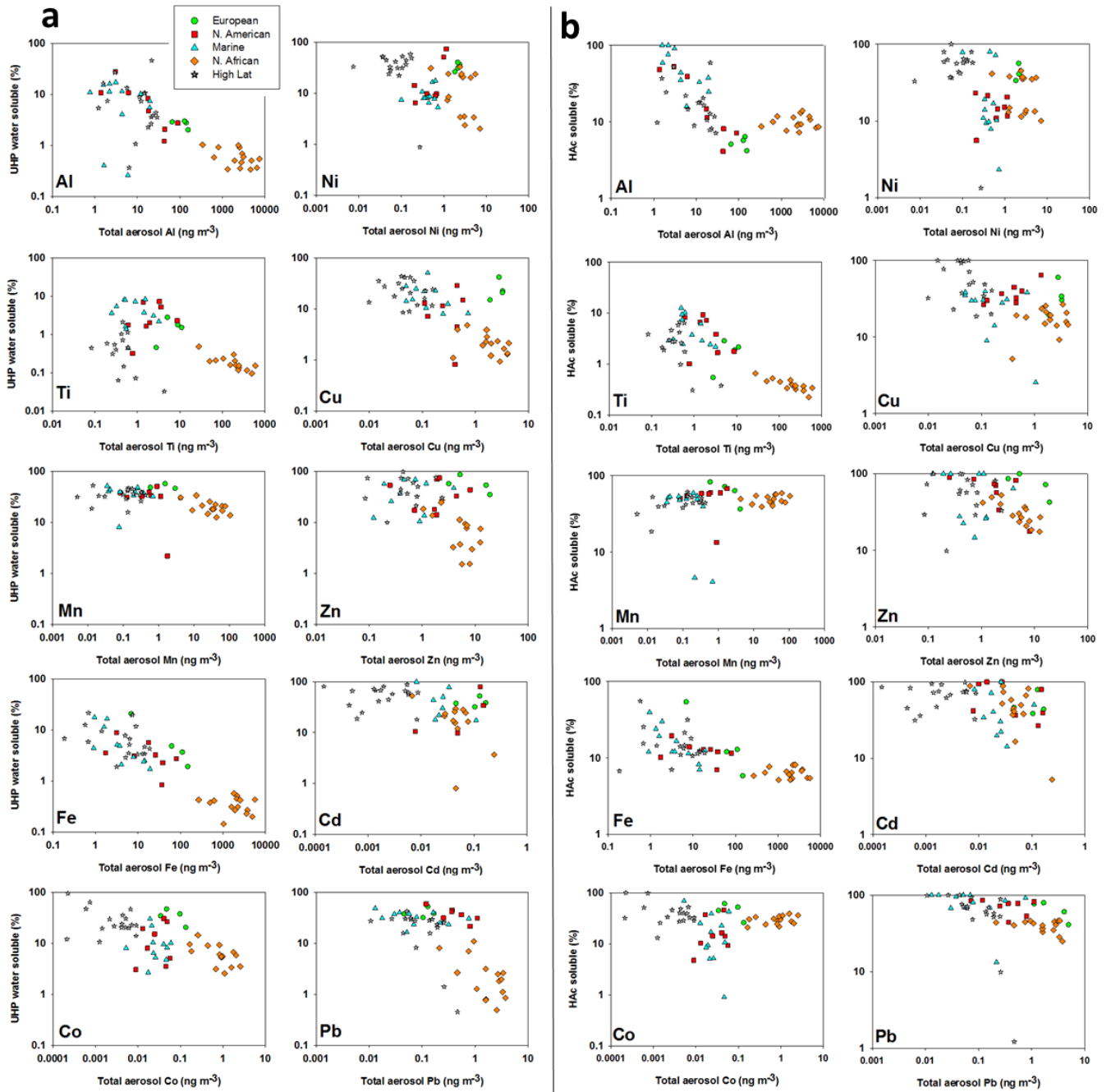
Figure 2

932
933
934



935
 936
 937
 938
 939
 940
 941
 942
 943
 944
 945
 946
 947

Figure 3



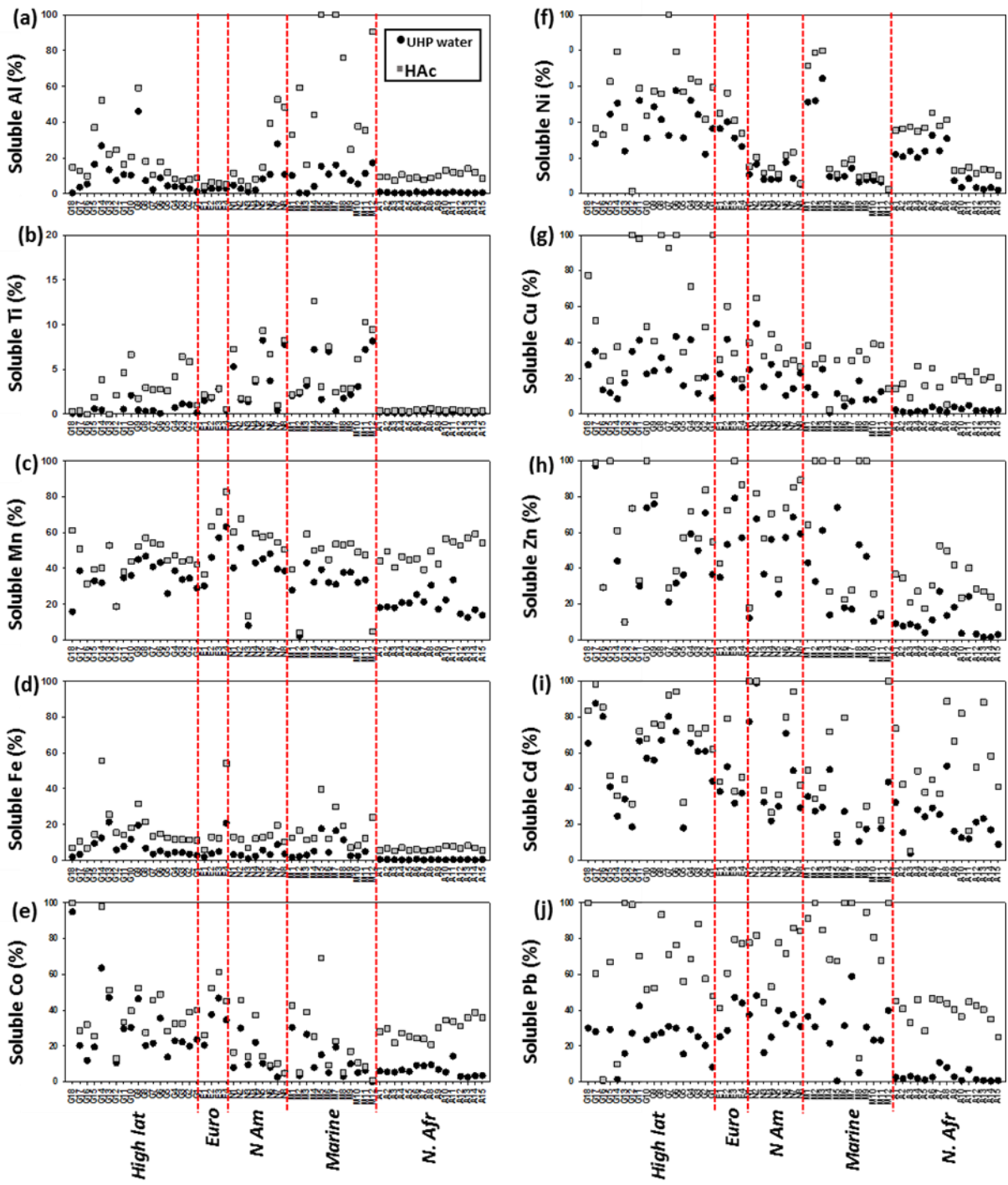
948

949

Figure 4

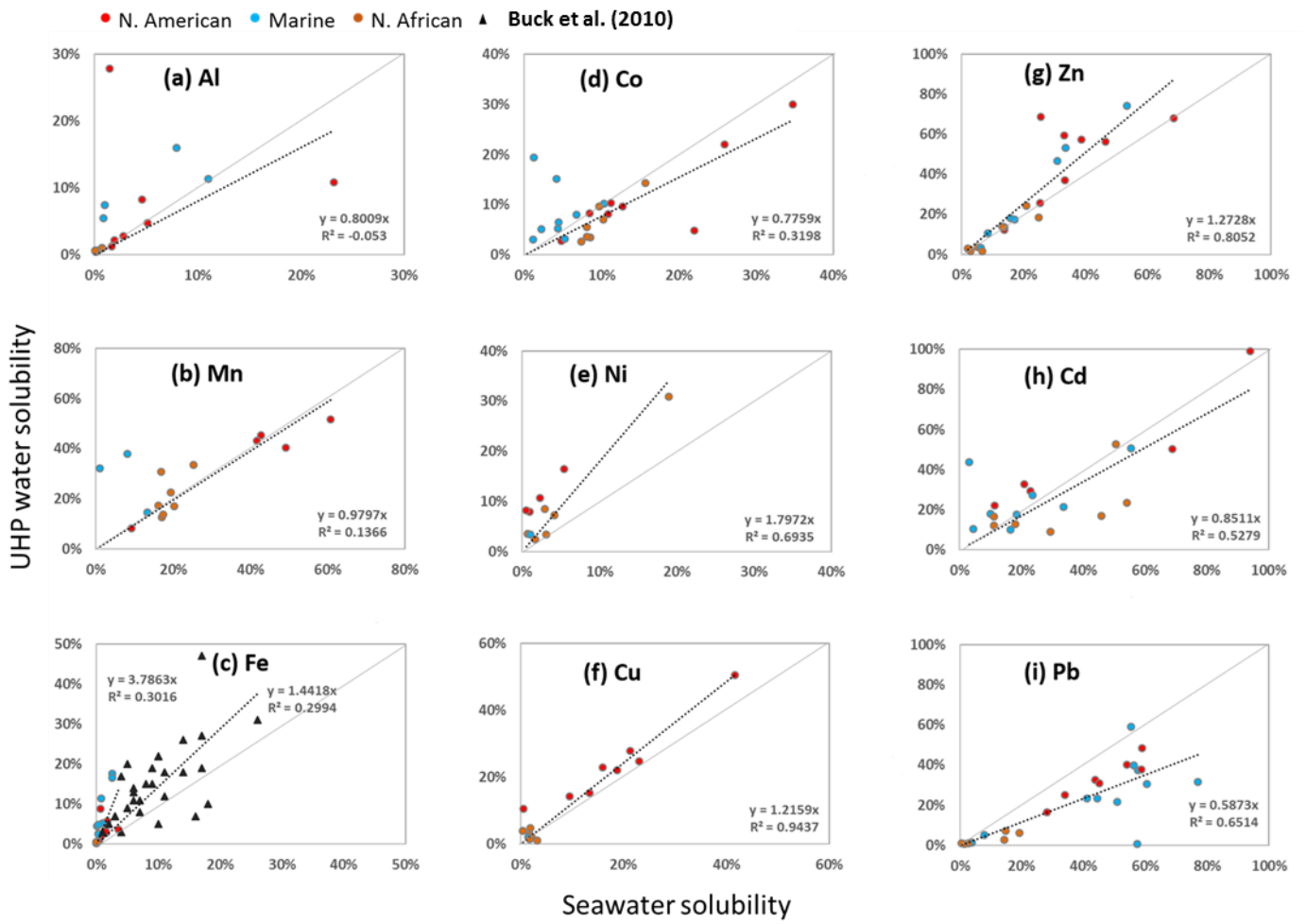
950

951



952

953 **Figure 5**



954

955

956

957 **Figure 6**

958

959

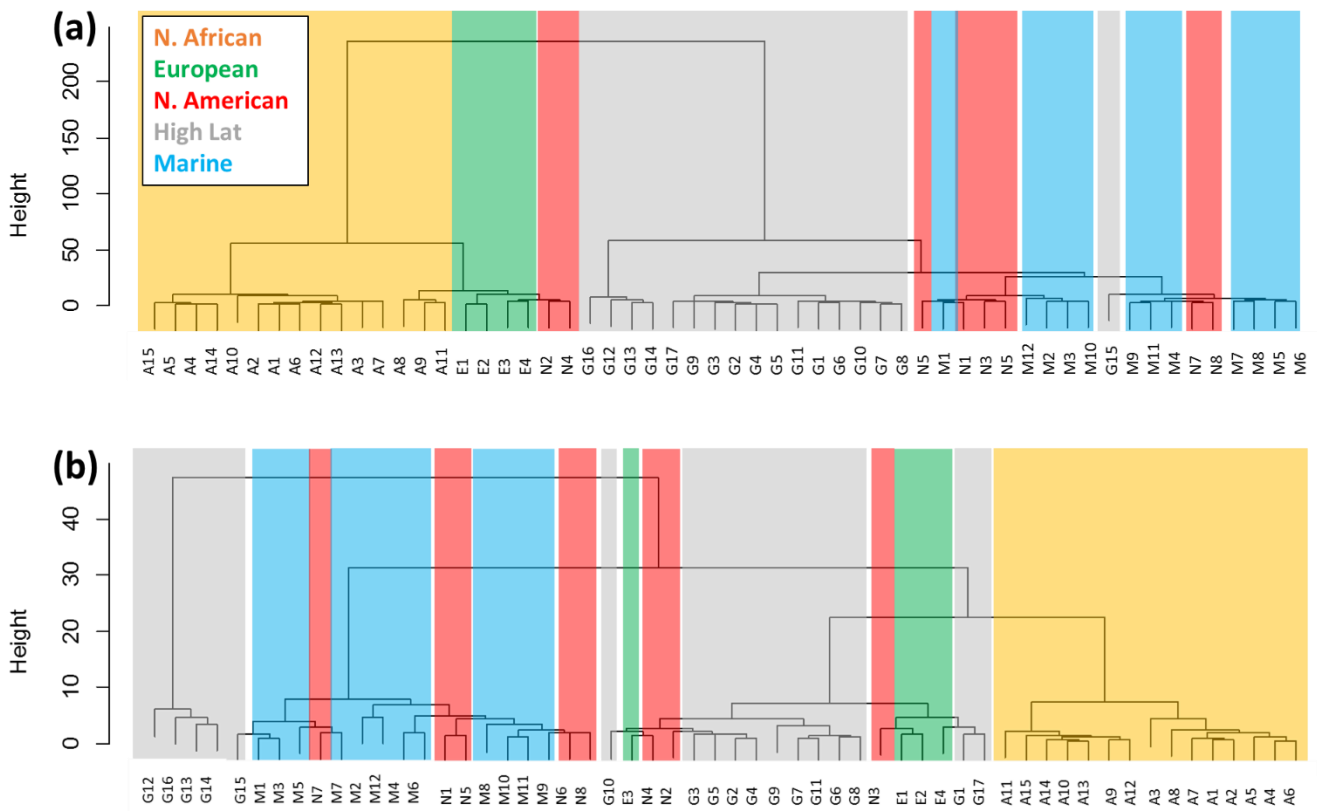
960

961

962

963

964



965
966
967
968

969
970
971
972
973
974
975
976

Figure 7

Captions: Figures

977
978
979 Figure 1. The GEOTRACES GA01 and GA03 cruise tracks (GA01, GA03-2010 and GA03-2011). In total, 57
980 aerosol samples (GA01 n = 18, GA03 n = 39; black dots) were collected. The samples are grouped by aerosol
981 source region (green = European (E1-4), blue = Marine (M1-12), yellow = North African (A1-15), red = North
982 American (N1-8), and grey = High Latitude (G1-18)), identified from air mass back trajectory simulations using
983 the NOAA ARL model, HYSPLIT (Stein et al., 2015; Rolph, 2017). Note that a different labelling convention
984 was used in Shelley et al. (2017) to refer to the GA01 samples. Here we use G1-18 to refer to the samples
985 collected during GA01 (A1-18 in Shelley et al., 2017), and A1-15 to refer to the North African samples from
986 GA03.

987
988 Figure 2. Total aerosol Fe and Al (ng m^{-3}) for: (a) all aerosol samples from cruises GA01 and GA03, (b)
989 samples from sources other than North Africa (i.e. the black diamonds in Fig. 2a), and (c) the samples inside the
990 dashed box in Fig. 2b. For High Latitude dust n = 18, European samples n = 4, North American samples n = 8,
991 Marine samples n = 12, and Saharan samples n = 15. Note error bars (standard deviations shown in Table S1)
992 are not included so as not to obscure the symbols.

993
994 Figure 3. Elemental mass ratios (normalised to Al) of total (black circles) and UHP water soluble (white
995 triangles) TEs. The UCC elemental ratio (Rudnick and Gao, 2003) is indicated by the solid horizontal line,
996 and the elemental ratio in North African sourced aerosols (Shelley et al., 2015) is indicated by the dashed horizontal

997 line on each plot. The red vertical lines separate the aerosol source regions, which are labelled in panel (a).
998 Samples G9-GA01 and M3-GA03 are indicated by blue arrows in panel c (see text for details).

999

1000 Figure 4. (a) Percentage of UHP water soluble TE (calculated from Eq. 1) versus total aerosol TE (ng m^{-3}), (b)
1001 percentage of 25 % acetic acid soluble TE (calculated from Eq. 2) versus total aerosol TE (ng m^{-3}). Data is
1002 plotted on log-log scales.

1003

1004 Figure 5. Solubility of Al, Ti, Mn, Fe, Co, Ni, Cu, Zn, Cd, Pb following a UHP water leach (UHP water, black
1005 circles, calculated using Eq. 1), and a sequential leach of 25 % acetic acid (HAc, grey squares, calculated using
1006 Eq. 2). The red vertical dashed lines represent the different aerosol source categories, as labelled in panel (b).
1007 Note that Ti (panel b) is highly insoluble and has a maximum value of <13%. The data for this figure is also
1008 presented in Fig. S4 as biplots of UHP water fractional solubility versus 25 % acetic acid fractional solubility.

1009

1010 Figure 6. Comparison of TE solubility following instantaneous leaches using UHP water or locally-collected,
1011 filtered seawater. The solid line is the 1:1 line. Where fewer data are observed, concentrations were below
1012 detection for one or both of the two leaches. The data for soluble aerosol Fe from within our study region from
1013 Buck et al. (2010) are plotted as black triangles in panel (c).

1014

1015 Figure 7. Heirachical cluster analysis of (a) log transformed total TE concentration data plus NO_3^- , and (b) log
1016 transformed fractional solubility following the two-step sequential leach (fractional solubility calculated using
1017 Eq. 2). The coloured blocks correspond with the aerosol source regions shown in the legend.

1018

1019

1020

1021